Physics – Uspekhi **47** (7) 687 – 704 (2004)

REVIEWS OF TOPICAL PROBLEMS PACS numbers: **42.55. – f**, **42.62. – b**, 42.65.Ky, 42.65.Re

Femtosecond pulses in nanophotonics

A A Ivanov, M V Alfimov, A M Zheltikov

DOI: 10.1070/PU2004v047n07ABEH001811

Contents

Abstract. We give an overview of the physical fundamentals of femtosecond nanophotonics — the basic physical phenomena behind the interaction of ultrashort laser pulses with nanoscale objects, nanocomposite materials, supramolecular structures, and molecular aggregates. Femtosecond laser pulses pave a way to achieving high intensities of electromagnetic radiation without irreversible damage to materials, making it possible to observe unique regimes of interaction of the light field with nanostructures and molecular aggregates. Dielectric and electron confinement, as well as resonances due to quantum size effects and collective phenomena in supramolecular and aggregate structures, radically enhance nonlinear-optical interactions of ultrashort pulses. These phenomena offer interesting solutions for a high-sensitivity nonlinear-optical metrology of nanostructured materials, including the analysis of their composition, structure, and morphology, suggesting new attractive strategies for the control, switching, and transformation of ultrashort pulses.

A A Ivanov, M V Alfimov Center of Photochemistry,
Russian Academy of Sciences,
ul. Novatorov 7a, 119421 Moscow, Russian Federation
Tel. (7-095) 935 02 09. Fax: (7-095) 936 12 55
E-mail: ivanov@photonics.ru
A M Zheltikov Physics Department, International Laser Center,
M V Lomonosov Moscow State University,
Vorob'evy gory, 119899 Moscow, Russian Federation
Tel. (7-095) 939 51 74. Fax: (7-095) 939 31 13
E-mail: zheltikov@top.phys.msu.su

Received 28 January 2004
Uspekhi Fizicheskikh Nauk **174** (7) 743 – 763 (2004)
Translated by A M Zheltikov; edited by A Radzig

1. Introduction

The development of natural sciences gives rise to new directions and areas of interdisciplinary research integrating advances in fundamental science and achievements of modern technologies. Impressive progress has been achieved over the past few years in working out the strategies to control the basic processes (including ultrafast phenomena) in matter by nanostructuring [1 – 3], as well as by engineering supramolecular structures and molecular aggregates [4, 5]. The preparation of new organic materials with high optical nonlinearities [6 – 19], unique nanocomposite materials for optics [20], and structures with optical properties controlled by quantum size effects [20 – 24] open the way for devising the highly efficient devices for frequency conversion and laser radiation control, including switches, gates, limiters, and frequency converters for ultrashort light pulses. In fact, we are witnessing the origination of a new field of research — femtosecond nanophotonics. Progress in this direction leads to revolutionary changes in ultrafast and nonlinear optics, quantum and atomic physics, chemical technologies, and biophotonics, providing deeper insights into the fundamental aspects related to the interaction of ultrashort waveforms of electromagnetic radiation with nanostructured matter.

Femtosecond laser pulses provide an opportunity to achieve high intensities of electromagnetic radiation without irreversible damage to materials, leading to unique regimes of interaction of the light field with nanostructures and molecular aggregates. Dielectric and electron confinement, as well as resonances due to quantum size effects and collective phenomena in supramolecular and aggregate structures, radically enhance nonlinear-optical interactions of ultrashort pulses. These phenomena open up fresh

opportunities for a high-sensitivity nonlinear-optical metrology of nanostructured materials, including the analysis of their composition, structure, and morphology, thus mapping out new attractive strategies for the control, switching, and transformation of ultrashort pulses.

In this paper, we provide an overview of the field of femtosecond nanophotonics and discuss the main physical processes behind interesting scenarios of interaction of ultrashort laser pulses with nanoscale objects, nanocomposite materials, supramolecular structures, and molecular aggregates. Section 2 is devoted to the generation of ultrashort pulses by laser systems of a new class — femtosecond chromium forsterite lasers with a regenerative amplification. Due to the unique combination of parameters of their laser pulses [25, 26], lasers of this type offer new solutions for the nonlinear-optical metrology of nanostructures [27 – 32], molecular aggregates [33], and optical microexplosions in solids [34] and hold much promise for biomedical applications [35 – 37].

In Section 3, we discuss applications of nonlinear-optical processes, enhanced by resonances related to collective phenomena in supramolecular structures, for the visualization of molecular aggregation. Nonlinear-optical manifestations of electron confinement in nanostructures are analyzed in Section 4, which is focused on optical harmonic generation in carbon nanotubes. Nonlinear-optical phenomena enhanced by dielectric confinement are illustrated by experiments on second- and third-harmonic generation in polymer films doped with silicon carbide nanocrystals (Section 5). In Section 6, we briefly outline new strategies offered by femtosecond pulses in biomedicine and biophotonics. Results of our analysis are summarized in the Conclusions.

2. Femtosecond chromium forsterite lasers

2.1 Generation of ultrashort pulses by mode-locked chromium forsterite lasers with regenerative amplification

Mode-locked chromium forsterite lasers with regenerative amplification constitute a new class of sources of ultrashort pulses possessing a unique combination of parameters of light pulses. These lasers open new horizons in the spectroscopy of ultrafast processes [39], nonlinear optics [40 – 44], optical metrology [45, 46], optics of nanostructures [27 – 32, 47, 48], and biomedical optics. Lasers of this class can generate light pulses with a duration of 50 – 150 fs, a wavelength of 1.2 – 1.3 μm, and a pulse power of a few gigawatts (Table 1). Femtosecond pulses of radiation in this spectral range make it possible to study ultrafast processes within the transparency band of many semiconducting materials, including silicon and its compounds, as well as gallium arsenide and gallium phosphide [49]. Radiation wavelengths of Cr:forsterite lasers are close to the point of zero group-velocity dispersion of standard fused silica fibers, giving rise to essential regimes of waveguide propagation and nonlinear-optical interactions of ultrashort pulses [45, 46]. Femtosecond pulses of Cr:forsterite-laser radiation also provide a convenient tool for studying resonances related to collective phenomena in supramolecular nanostructures [33] and quantum size effects in systems of nanotubes [29, 30]. Such pulses also permit a search for new solutions to the problems of ultrafast [50] and nonlinear [40 – 44] optics and laser biomedicine [35 – 38, 51]. Parameters of the main types of Cr:forsterite laser systems with regenerative amplification, elaborated by different research groups [40 – 42, 52 – 55], are summarized in Table 1.

Table 1. Parameters of Cr:forsterite laser systems with regenerative amplification using different types of electro-optical switches

Year	1998	1998	1999	1999	2000
Pulse repetition rate, Hz	1000	1000	1000	10	1000
Radiation wavelength of the master oscillator, nm	1255	1220	1250	1280	1250
Radiation wavelength of the regenerative amplifier, nm	1255	1220	1250	1240	1230
Pulse duration, fs	150	54	135	77	75
Pockels cell	$LiNbO_3$	DKD*P	BBO	DKD*P	DKD*P
Pump radiation energy, mJ	7	10	5	140	8
Output energy, μJ	30	50	200	400	100
Losses per single pass through the Pockels cell, %	< 2	15	2.5	> 12	12
Pulse compression efficiency, %	30	25	65	50	50
References	[52]	[53]	[54]	[55]	[28 – 34]

The femtosecond chromium forsterite laser system developed and created at the Center of Photochemistry, Russian Academy of Sciences, comprises a Cr^{4+}:forsterite master oscillator (Fig. 1), a stretcher, an optical isolator, a regenerative amplifier, and a compressor (Fig. 2). The master oscillator, pumped with an ytterbium fiber laser, generates 40-fs light pulses with a repetition rate of 120 MHz. The central wavelength of this laser radiation is 1250 nm with a bandwidth of 40 nm and a mean output power of about 180 mW.

Horizontally polarized 40-fs pulses are then stretched up to 140 ps in a grating stretcher (Fig. 2). Upon passing through a Faraday isolator and a $\lambda/4$ plate, the light pulses became vertically polarized. These pulses were then transmitted through a broadband polarizer, to be injected in the regenerative amplifier at the points in time corresponding to maximum population inversion induced by pump pulses with a repetition rate of 1 kHz. An optical switch is used to set a horizontal polarization of pulses injected into the cavity of the amplifier. An amplified pulse with an energy of 100 μJ was coupled out of the amplifier through the switch triggered at the instant of time corresponding to optimal amplification. Radiation coming out of the amplifier is vertically polarized again. The amplified pulse was returned to the isolator along the same optical path. Radiation passing through the isolator in the backward direction experiences no change in its polarization since polarization rotations introduced by the $\lambda/4$ plate and the Faraday isolator compensate for each other. The pulses coupled out of the isolator through the broadband polarizer were transmitted through a $\lambda/2$ plate and recompressed to a 75-fs duration in a grating compressor. Approximately 50% of pulse energy was lost at this stage.

Modeling of the regenerative amplification stage in a chromium forsterite laser system and analysis of the para-

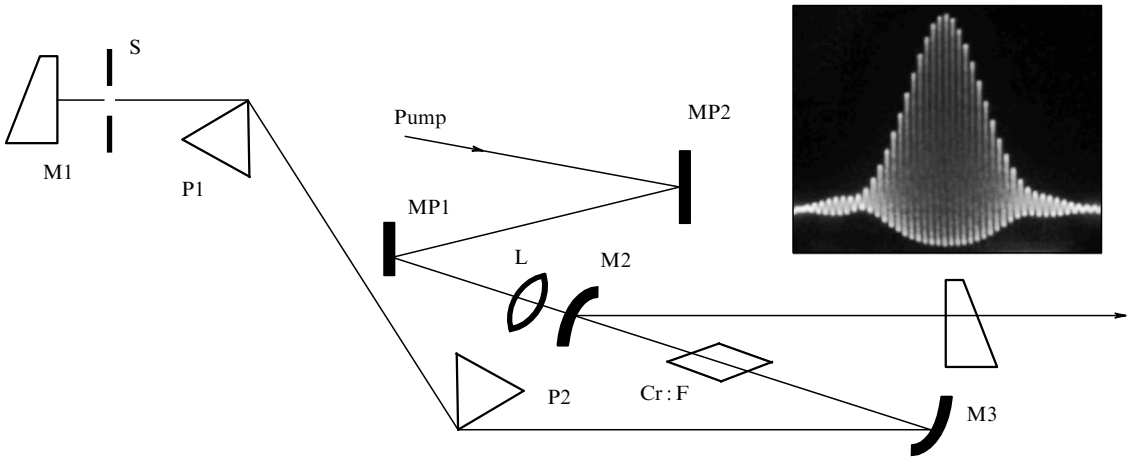

Figure 1. Schematic diagram of the master oscillator of the femtosecond Cr:forsterite laser: MP1, MP2, pump mirrors; L, pump lens; M1 – M4, cavity mirrors; P1, P2, cavity prisms; Cr:F, Cr^{4+}:Mg_2SiO_4 crystal, and S, intracavity slit. The inset shows an autocorrelation trace of a 30-fs output pulse from the Cr:forsterite master oscillator.

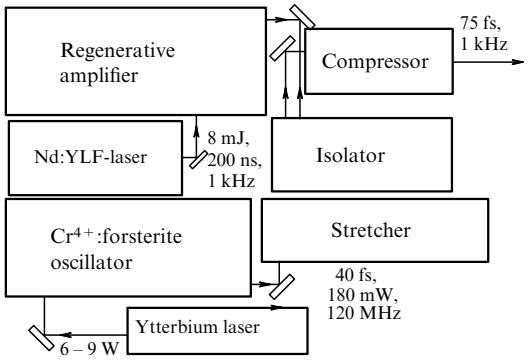

Figure 2. Diagram of the femtosecond Cr:forsterite laser system with a regenerative amplifier.

meters of the available femtosecond lasers of this class (see Table 1) show that such systems can generate amplified femtosecond pulses with energies in the submillijoule range. One of the main factors limiting the energy of laser pulses in such systems is associated with radiation absorption in the KD*P crystal in the Pockels cell of the regenerative amplifier. This effect also leads to a frequency shift of amplified femtosecond pulses. Femtosecond laser pulses of mode-locked chromium forsterite laser systems with regenerative amplification allow high intensities of electromagnetic radiation to be achieved without irreversible damage to materials, paving the ways to observe unique regimes of interaction of the light field with nanostructures and molecular aggregates.

2.2 Frequency conversion of femtosecond chromium forsterite laser pulses

In this section, we discuss the possibility of highly efficient frequency conversion of femtosecond Cr:forsterite-laser pulses and generation of frequency-tunable radiation within the wavelength range of 350 – 600 nm through nonlinear-optical spectral transformations of ultrashort laser pulses in microstructured fibers. Propagation of 75-fs 10 – 200-nJ Cr: forsterite-laser pulses through microstructured and tapered fibers is accompanied by cascaded four-wave mixing, giving rise to manifold new spectral components in a broad visible region and substantial spectral broadening within the wavelength range from 1300 up to 1600 nm.

Frequency conversion of femtosecond laser pulses constitutes one of the urgent problems of laser physics and quantum electronics. The standard solution to this problem is to use nonlinear-optical crystals [56]. Frequency-conversion capabilities of nonlinear crystals can be extended in certain cases by periodic poling, allowing quasi-phase matching of nonlinear-optical interactions [57, 58]. The potential of photonic crystals for the frequency conversion of ultrashort pulses has been recently demonstrated, and several attractive recipes for the phase matching of nonlinear-optical processes have been suggested [59 – 61]. The main factors limiting the efficiency of frequency conversion of ultrashort pulses in nonlinear crystals and periodic structures include group-velocity dispersion and the restricted spectral range of phase matching.

Microstructured [62 – 68] and tapered [46, 69] fibers possess several remarkable and unique properties allowing highly efficient nonlinear-optical interactions to be implemented even for low-power ultrashort laser pulses. In particular, dispersion of such fibers can be tailored by changing their geometry [70]. A high refractive-index step between the core and the cladding, attainable with such fibers, strongly confines the electromagnetic radiation field to the fiber core [71, 72]. Microstructured and tapered fibers offer much flexibility in phase-matching the third-harmonic generation (THG) [73 – 75] and four-wave mixing [76], allowing both radiation with a very broad spectrum (supercontinuum) [77] and isolated spectral components [76, 78, 79] to be generated with high efficiency.

Experiments [40 – 46, 80, 81] have shown that nonlinear-optical interactions in microstructured and tapered fibers may result in highly efficient frequency conversion of femtosecond Cr:forsterite-laser pulses. Experiments on frequency conversion of femtosecond Cr:forsterite-laser pulses were performed with a family of fused silica microstructured fibers where the cladding, consisting of one, two, or more hexagonal cycles of air holes, surrounds the central fiber core with a diameter of a few micrometers (the inset to Fig. 3). Microstructured fibers were fabricated of fused silica using the technology described in detail elsewhere [82, 83]. The minimal core diameter in the fabricated family of fibers was

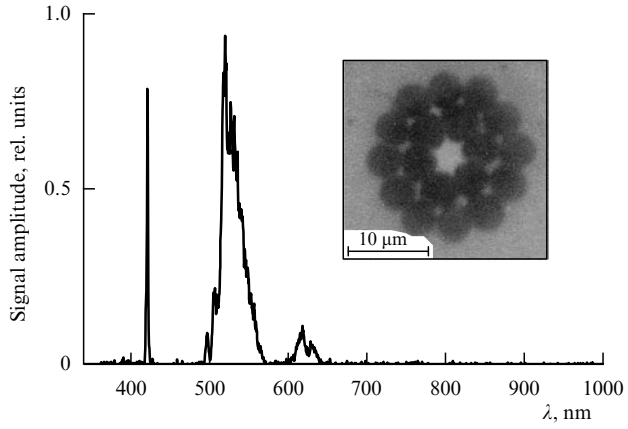

Figure 3. Generation of an anti-Stokes signal and the third harmonic in the central core of a microstructured fiber with a diameter of 3 μm. The inset shows a cross-section image of a microstructured fiber with two cycles of air holes around the central waveguiding core.

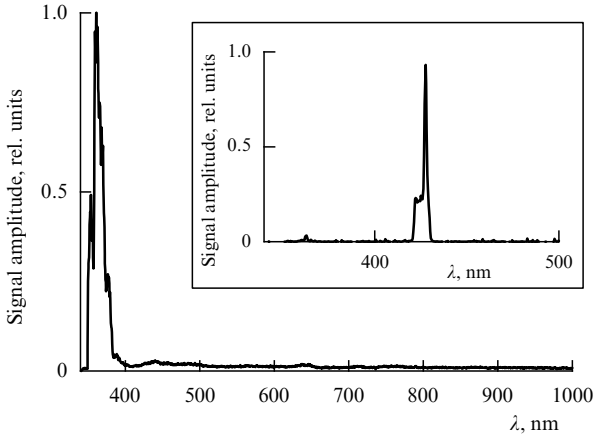

Figure 4. Generation of a high-frequency spectral component with a wavelength around 370 nm in a submicron threadlike waveguide channel of a microstructured fiber. The fiber length is 7 cm. The energy of laser pulses coupled into the fiber is about 50 nJ. The inset shows the spectrum of the third harmonic of pump radiation generated in submicron threadlike waveguide channels of the microstructured fiber.

equal to 1 μm. The air-filling fraction of the microstructured part of the cladding in the created fibers, as can be seen from the inset to Fig. 3, is very large, providing a high refractive-index step between the core and the cladding in the fiber and strongly confining the light field in the fiber core. An array of submicron-sized fused silica channels in the form of threads, bounded by the system of air holes in the fiber cladding, serves as additional multiple cores of the fiber. These submicron cores provide a high degree of light confinement due to the high refractive-index step and allow waveguide enhancement factors, close to the physical limit determined by the competition of diffraction and refractive-index-step waveguiding, to be achieved for nonlinear-optical processes [84, 85]. Microstructured fibers with one, two, and three cycles of air holes surrounding the central core were employed for the frequency conversion of femtosecond Cr:forsterite-laser pulses.

The microstructured fiber design considered integrates several small-core high-refractive-index-step fibers into a bundle. Such a fiber can be made as long as several hundred meters, thus permitting length limitations, typical of tapered fibers due to technical problems in their fabrication and use, to be overcome by means of fiber microstructuring. The fact that the microstructure-integrated bundle includes submicron fused-silica waveguiding threads with different sizes helps to achieve wavelength tunability in the frequency conversion of ultrashort pulses (femtosecond pulses of a Cr:forsterite laser in our experiments).

Radiation generated by the Cr:forsterite laser system was coupled into the central core or one of the threadlike fused silica channels (see the inset to Fig. 3) in a microstructured fiber. The duration of laser pulses at the input of microstructured fibers was about 150 fs. Propagation of femtosecond laser pulses through microstructured fibers was accompanied by nonlinear-optical interactions giving rise to new frequency components in the spectrum of radiation coming out of the fiber. Parametric four-wave mixing of the $2\omega_p = \omega_s + \omega_a$ type (ω_p is the frequency of pump radiation, and ω_s and ω_a are the frequencies of the Stokes and anti-Stokes signals, respectively) in the central fiber core resulted in the efficient generation of an anti-Stokes component centered around 530 nm with a spectral bandwidth of about 35 nm (Fig. 3). Phase matching for such processes in microstructured fibers was analyzed in earlier works [76, 79, 86]. We also observed efficient generation of the third harmonic of pump radiation with the amplitude of the third harmonic comparable to the amplitude of the anti-Stokes signal (see Fig. 3).

Nonlinear-optical spectral transformation of femtosecond Cr:forsterite-laser pulses in submicron fused-silica waveguiding channels of different diameters resulted in the generation of new frequency components within a broad spectral range (Fig. 4). The wavelength range where the efficiency of nonlinear-optical frequency conversion reaches its maximum is determined by the dispersion properties of the waveguide channel. The size of the channel is thus the key parameter controlling the process of nonlinear-optical frequency conversion. The possibility of tuning the frequencies of new spectral components generated by femtosecond Cr:forsterite-laser pulses in submicron fused-silica channels of different diameters is illustrated in Fig. 4. Effective cascading of nonlinear-optical processes in submicron waveguiding channels leads, as can be seen from Fig. 4, to the generation of the frequency component with a central wavelength around 370 nm and a spectral bandwidth of about 30 nm (the wavelength of the third harmonic runs to 420 nm for a Cr:forsterite-laser radiation). This process increases the carrier frequency of femtosecond Cr:forsterite-laser pulses by more than 580 THz. The efficiency of this frequency-conversion process was as high as several percent, giving rise to blue light easily seen by the naked eye on a white screen.

Cross-correlation frequency-resolved optical gating (XFROG) [87] was applied in experiments [39] to characterize anti-Stokes pulses generated in the microstructured fiber. An XFROG signal was produced in those experiments by mixing the anti-Stokes signal E_a from the fiber with the second-harmonic output E_a of the Cr:forsterite laser in a BBO crystal. A two-dimensional XFROG spectrogram

$$S(\omega,\tau) \propto \left| \int_{-\infty}^{\infty} E_a(t)\, E_{SH}(t-\tau)\, \exp(-i\omega t)\, dt \right|^2$$

was then plotted in a standard way by measuring the XFROG signal as a function of the delay time τ between

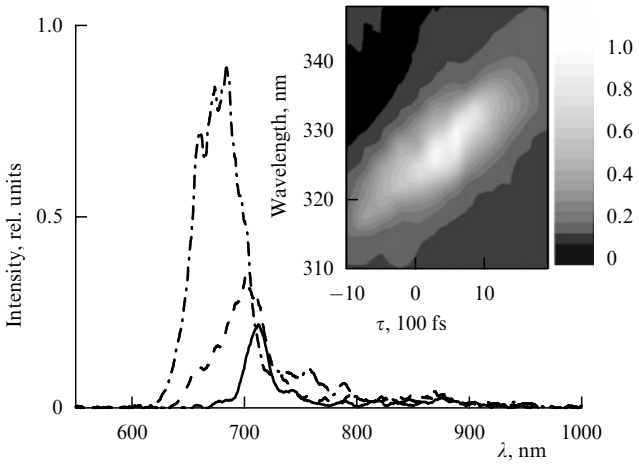

Figure 5. The spectrum of the anti-Stokes signal generated in a microstructured fiber by Cr:forsterite-laser pulses of 1.24-μm radiation with an input energy of 200 nJ (solid line), 250 nJ (dashed line), and 275 nJ (dot-and-dash line). The inset shows the intensity of the sum-frequency signal generated in a BBO crystal by the second-harmonic pulse from the Cr:forsterite laser and the anti-Stokes pulse from the microstructured fiber as a function of the wavelength and the delay time τ between the second-harmonic and anti-Stokes pulses.

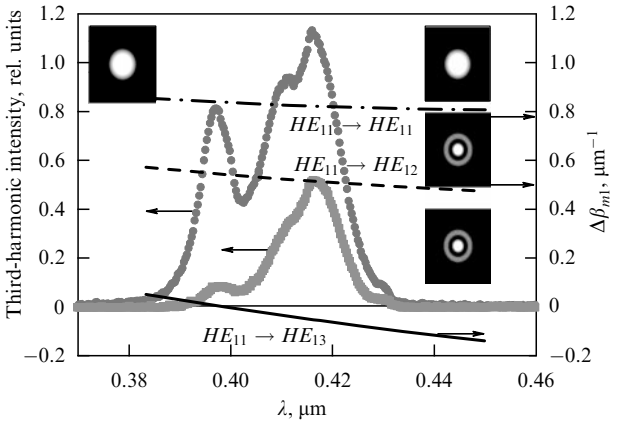

Figure 6. Spectra of the third harmonic produced in a tapered fiber by Cr:forsterite-laser pulses of 1.25-μm radiation with an initial duration of 30 fs. The energy of pump laser pulses is 0.24 nJ (bold solid curve) and 0.32 nJ (dotted line). Also shown are the values of $\Delta\beta_{m1}$, the mismatch of propagation constants for the HE_{11} mode of the pump pulse and the HE_{1m} mode of the third harmonic, calculated for a fiber consisting of a fused silica core with a diameter of 2.6 μm and an air cladding: $m = 1$ (dot-and-dash curve), $m = 2$ (dashed curve), and $m = 3$ (thin solid curve). The insets show transverse intensity distributions of light field in HE_{1m} modes ($m = 1, 2, 3$) of the tapered fiber, illustrating the $HE_{11} \rightarrow HE_{1m}$ transformation of the spatial modes corresponding to the third-harmonic generation process.

the second-harmonic and anti-Stokes pulses and spectrally dispersing the XFROG signal. The XFROG spectrogram visualizes the temporal envelope, the spectrum, and the chirp of the anti-Stokes signal generated in the microstructured fiber. The inset to Fig. 5 presents an XFROG spectrogram of the anti-Stokes signal generated in the microstructured fiber within the wavelength range of 650–730 nm (Fig. 5). The spectrogram was measured with the use of 620-nm 90-fs second-harmonic pulses. As can be seen from this map, the anti-Stokes pulse has a duration on the order of 1 ps, a smooth temporal envelope, and a virtually linear positive chirp.

Different frequency components of the anti-Stokes pulse generated and shaped in the microstructured fiber are characterized by various group delays. The instantaneous frequency ω in this pulse, as can be seen from the results presented in the inset to Fig. 5, is related to the delay time τ by a one-to-one mapping defined by the pulse chirp. Such a one-to-one $\tau - \omega$ mapping allows spectral measurements to be performed by varying the delay time between the pump pulses [88–91]. In experiments [39], a linearly chirped anti-Stokes pulse from a microstructured fiber was employed as one of the biharmonic pump fields for the spectroscopy of coherent anti-Stokes Raman scattering (CARS).

Thus developed microstructured fiber design allows femtosecond Cr:forsterite-laser pulses to be frequency-converted to the spectral range that is of special interest and importance for photochemical and photobiological studies, enhancing the capabilities of femtosecond Cr:forsterite lasers in femtosecond spectroscopy and time-resolved measurements, as well as extending the applicability area of such laser systems to the control of ultrafast processes in physics, chemistry, and biology.

The results of experiments [40–42, 45, 46] have demonstrated a highly efficient frequency conversion of femtosecond Cr:forsterite-laser pulses through direct and cascaded four-wave mixing processes in tapered fibers. In particular, unamplified 30-fs Cr:forsterite-laser pulses were utilized to generate the third harmonic in the phase-matching regime (Fig. 6). Propagation of 75-fs 10–200-nJ Cr:forsterite-laser pulses through a tapered fiber in the range of anomalous dispersion is accompanied by multiple phase-matched cascaded four-wave mixing giving rise to a manifold of new spectral components in the visible range (Fig. 7a) and resulting in a considerable spectral broadening in the infrared range of wavelengths from 1300 to 1600 nm (Fig. 7b). Tapered-fiber-based components for the spectral transformation of ultrashort light pulses may thus substantially expand the capabilities of femtosecond Cr:forsterite lasers, allowing ultrashort pulses of these lasers to be used for the solution of a broad class of fundamental and applied problems in spectroscopy, telecommunication technologies, coherent and quantum control, absolute-phase measurements for few-cycle pulses, and biomedicine.

3. Visualization of J-aggregation with two-photon-resonance-enhanced third-harmonic generation

In this section, we will show that third-harmonic generation (THG) enhanced due to a two-photon resonance provides a high level of nonlinear signal from the bulk of a solution of J-aggregating ethyl thiacarbocyanine molecules. Third-harmonic generation under these conditions is free of one-photon absorption of pump radiation and nonlinear signal, which makes it possible to use this process for the metrology of nonlinear-optical properties of bulk samples, as well as for the control and visualization of the aggregation process with a high temporal and spatial resolution. We will demonstrate the emergence of correlations between the third-harmonic signal and two-photon-excited laser-induced fluorescence (LIF). Third-harmonic generation will be shown to be ideally suited as a local probe for J-aggregating solutions, which is sensitive to the structure and sizes of J-aggregates.

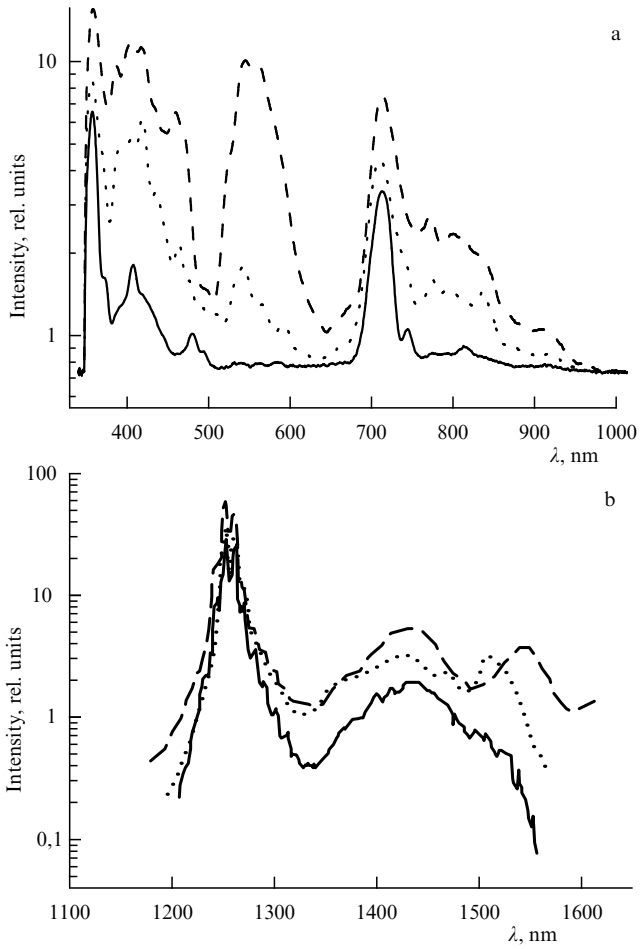

Figure 7. Spectra of radiation at the output of a tapered fiber with a taper-waist diameter of 2 μm measured in the wavelength ranges of (a) 350 – 950 nm, and (b) 1200 – 1600 nm. The energy of 75-fs Cr:forsterite-laser pulses coupled into the fiber is 100 nJ (solid line), 150 nJ (dotted line), and 200 nJ (dashed line).

3.1 New materials for optical technologies and J-aggregates

Synthesis of new materials for optical technologies is one of the key problems of physical chemistry. Investigations of structure – optical property relations for chemical substances have culminated in the past few years in impressive progress in the development of physical and chemical principles for the production of new materials with strong optical nonlinearities [6 – 11] for optical data processing, switching, multiplexing and demultiplexing, filtering, logic gating, and nonlinear-optical frequency conversion [12 – 16]. These studies resulted in a theoretical substantiation and experimental implementation of conceptually new approaches to the architecture of molecular compounds, permitting synthesis of materials with desirable and controllable nonlinear-optical properties [17, 18], thus opening new horizons in optical technologies, ultrafast photonics, optical data transmission and data processing, and laser physics. These new approaches integrate novel chemical-engineering strategies and physical methods, including creation of functional chemical groups [4, 19] where electrons are delocalized along the molecular core [11], utilization of strong optical nonlinearities of molecular aggregates [5, 92 – 94] and spatially arranged (e.g., chiral) supramolecular structures [4], as well as the enhancement of optical nonlinearities due to local-field effects using the methods of nano-optics and nanophotonics [95].

Metrology of nonlinear-optical properties of new materials for optical technologies is often grounded on the *z*-scan technique [95] or degenerate four-wave mixing [96, 97], including time-resolved pump – probe measuring methods [96, 98]. Frequency-degenerate nonlinear-optical processes can provide valuable information about the real and imaginary parts of the third-order nonlinear-optical susceptibility, which is necessary for the analysis of potential applications of new materials with strong nonlinearities, specifically supramolecular structures and J-aggregates [5, 99 – 104]. Such techniques usually comprise measurements in the regime of one-photon resonances. Strong one-photon absorption often complicates studies of bulk samples under these conditions. Much of the information related to the aggregation of molecules and formation of nano- and microcrystallites in the bulk of aggregating solutions remains inaccessible to measuring instruments with such an approach.

Third-harmonic generation enhanced by two-photon resonance permits reaching a high level of nonlinear signal from the bulk of a solution of J-aggregating ethyl thiacarbocyanine molecules. Process of J-aggregation, discovered in the 1930s [105, 106], is typically observed in aqueous solutions of a certain type of dye. An increase in dye concentration in solution in the regime of J-aggregation gives rise to narrow absorption bands violet-shifted with respect to broader absorption bands inherent in lower-concentration solutions of the same dye. Research into J-aggregation is motivated by the possibilities of using aggregates of this type as sensitizers, as well as by unusual coherent phenomena and nonlinear-optical processes originating from collective states of delocalized electrons in J-aggregates [92 – 94]. Two-photon-resonance-enhanced THG represents an attractive technique for the metrology of nonlinear-optical properties of bulk J-aggregating solutions, as well as for the control and visualization of the aggregation process with a high temporal and spatial resolution. Experiments [33] have revealed correlations between the third-harmonic signal and that of two-photon-excited LIF. These correlations indicate that pump radiation selectively addresses J-aggregating molecules. The third-harmonic signal from J-aggregates displays interesting variations as a function of the temperature of the J-aggregating solution. The revealed correlations between changes in the absorption spectrum of a J-aggregating solution and the intensity of the third harmonic suggest the possibility of using THG as a local probe capable of on-line monitoring of J-aggregation in the bulk of a sample being heated.

3.2 Two-photon-resonant third-harmonic generation

Third-harmonic generation gives a classic example of nonlinear-optical interactions and one of the most extensively employed practical nonlinear-optical techniques [56, 107]. Third-harmonic generation offers ways for the frequency conversion of laser radiation [56, 108], nonlinear-optical diagnostics in the gas and condensed phases [107, 109], surface analysis, as well as three-dimensional microscopy of biological objects [110, 111] and laser-produced plasmas [34, 112].

The efficiency of THG is controlled by the third-order nonlinear-optical susceptibility of a medium, along with the phase matching and absorption of the pump and third-harmonic fields [108]. Third-harmonic generation enhanced by a two-photon resonance is at the heart of the method of

J-aggregation visualization proposed by Akimov et al. [33]. In contrast to one-photon resonances, THG enhancement due to a two-photon-resonant growth in the nonlinear-optical susceptibility does not lead to a dramatic increase in the absorption of pump radiation. With no resonance-enhanced one-photon absorption, efficient two-photon-resonant THG can give rise to a spatially resolvable nonlinear-optical signal from the bulk and extended media. This circumstance constitutes one of the main advantages of two-photon-resonant THG over techniques based on frequency-degenerate processes with one-photon resonances.

The intensity of pump radiation propagating along the z-axis in a nonlinear-optical medium with resonant two-photon absorption decreases as $I = I_0(1 + \omega\gamma I_0 z)^{-1}$ [56], where I_0 is the initial intensity of the pump field, and γ is the coefficient of two-photon absorption. This expression for radiation damping radically differs from the Bouguer–Lambert–Beer law, namely $I = I_0 \exp(-\alpha z)$, which governs the decay of radiation intensity due to one-photon absorption in a medium with an absorptance α. Since the quantity $\omega\gamma I_0 L$ (L is the length of the nonlinear medium) is usually small compared to unity, two-photon-absorption-induced losses can typically be tolerated in many nonlinear-optical experiments. Thus, two-photon resonances can provide high efficiencies of THG without the process becoming significantly lossy, allowing an efficient generation of spatially resolved third-harmonic signal from three-dimensional samples.

3.3 Visualization of J-aggregation using third-harmonic generation

Akimov et al. [33] studied J-aggregation for a water solution of pyridine salt of 3,3′ disulfopropyl 9-ethyl 4,5,4′,5′ dibenzothiacarbocyanine (the chemical structure of this molecule is depicted in Fig. 8). A specially designed cell allowed a controlled heating of the solution. Production of different forms of J-aggregates was accompanied by changes in absorption spectra of the solution and the appearance of characteristic red-shifted absorption peaks related to excitonic transitions and known as J-bands (see Fig. 8).

Femtosecond pulses of Cr:forsterite-laser radiation with a wavelength of 1.25–1.27 μm were used in our experiments as an optical pump. Laser radiation with these wavelengths meets the condition of a two-photon resonance for excitonic J-band transitions in J-aggregates within the range of 625–635 nm. The femtosecond regime of optical excitation, on the other hand, allows high intensities of laser radiation to be achieved with relatively low energy fluences, preventing laser-induced breakdown and minimizing effects related to heat-transfer processes. A Cr:forsterite laser is, therefore, ideally suited as a pump source for the diagnostics of J-aggregating ethyl thiacarbocyanine molecules using two-photon-resonant nonlinear-optical processes.

Radiation generated by the Cr:forsterite-laser system described in Section 2 of this review was focused onto the studied J-aggregating solution (Fig. 9). The third harmonic generated in this solution was detected simultaneously with the signal of two-photon-excited photoluminescence which was also induced by Cr:forsterite-laser radiation. Absorption spectra were measured with a Hitachi-330 spectrophotometer.

Third-harmonic generation enhanced by a two-photon resonance provides a high level of nonlinear signal from the bulk of the solution of J-aggregating ethyl thiacarbocyanine molecules. The efficiency of nonlinear-optical interactions in

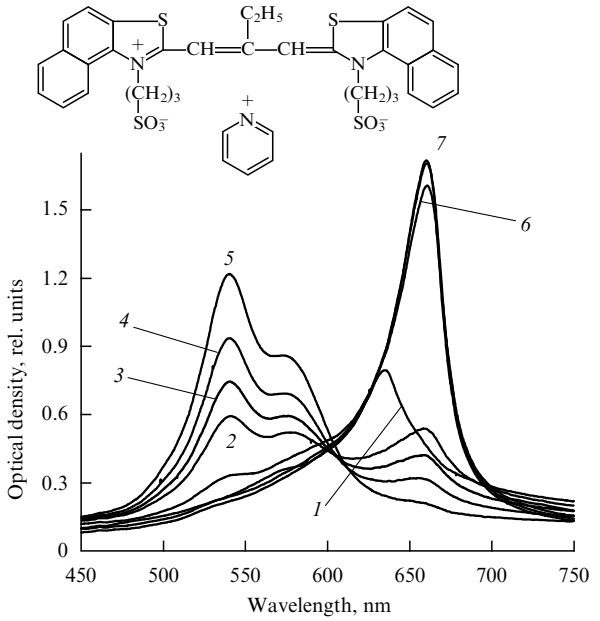

Figure 8. Transformation of the absorption spectrum of ethyl thiacarbocyanine in water heated from 1.4 up to 84 °C (curves *1–5*) and subsequently cooled down to 5 °C (curves *5–7*): (*1*) 1.4 °C, (*2*) 70 °C, (*3*) 75 °C, (*4*) 79 °C, (*5*) 84 °C, (*6*) 55 °C, and (*7*) 5 °C. As the temperature decreases, absorption in the J-peak centered at 658 nm increases, indicating the formation and stabilization of the relevant form of J-aggregates. The content of ethyl thiacarbocyanine in water solution amounts to 0.8 mg per 15 ml. The chemical structure of pyridine salt of 3,3′ disulfopropyl 9-ethyl 4,5,4′,5′ dibenzothiacarbocyanine is shown at the top.

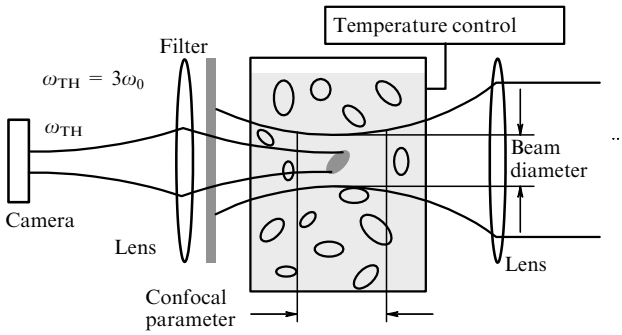

Figure 9. Diagram of third-harmonic generation in a controllably heated J-aggregating solution.

the field of femtosecond Cr:forsterite-laser pulses was sufficient to visually observe the third-harmonic signal, with an appropriate spectral filtering, on a white screen or to reliably detect this signal in broad pump beams with a photo or video camera. Third-harmonic beam patterns recorded with a video camera are presented in Fig. 10. Third-harmonic generation under conditions of a two-photon resonance is free of strong exponential absorption, typical of one-photon resonances, which makes this technique an ideal probe for the metrology of nonlinear-optical properties of three-dimensional samples and on-line monitoring of the aggregation process with a high temporal and spatial resolution.

J-aggregation in a heated solution gives rise to random variations in the spatial distribution of the refractive index and the nonlinear-optical susceptibility, resulting in visible fluctuations of the intensity and the beam pattern of the third harmonic (cf. Figs 10a and 10b). These fluctuations may be a

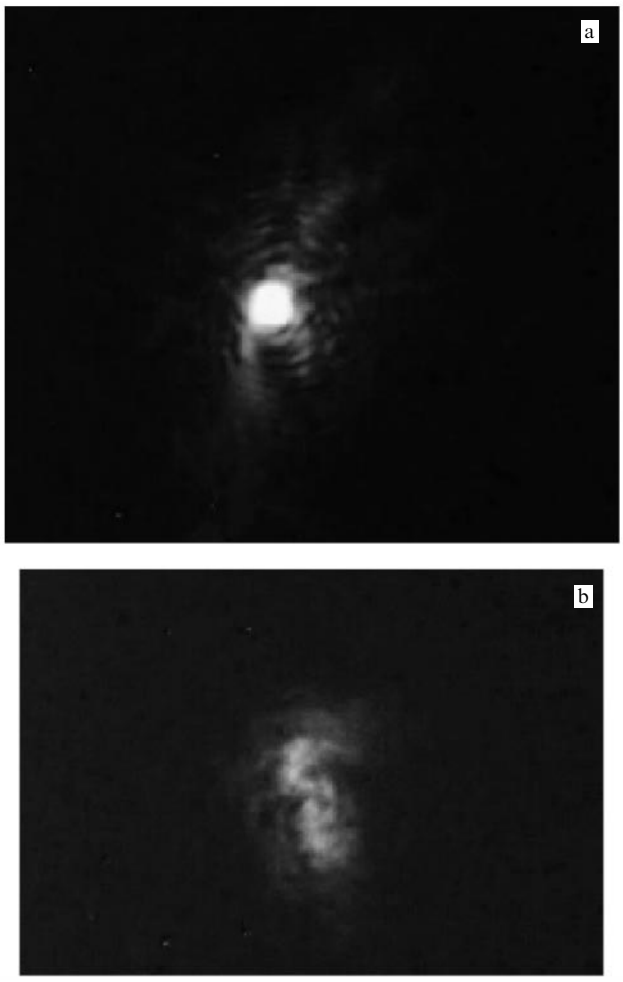

Figure 10. Images of the third-harmonic beam produced in a heated J-aggregating water solution of ethyl thiacarbocyanine recorded with a video camera (a) in an optically uniform solution, and (b) in a solution with optical inhomogeneities related to the flows of J-aggregating matter and microcrystals of J-aggregates. The waist diameter of the focused pump beam is 50 μm.

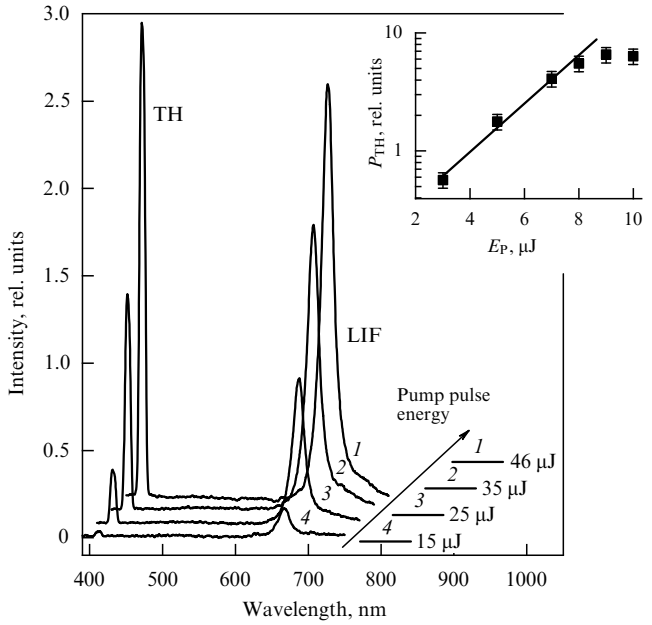

Figure 11. Correlated growth of third-harmonic (TH) and two-photon-excited photoluminescence intensities as functions of the pump pulse energy in a J-aggregating solution of ethyl thiacarbocyanine. The pump radiation wavelength is 1.26 μm. The inset shows the third-harmonic power P_{TH} measured as a function of the pump pulse energy E_p (squares with error bars). The solid line represents the cubic scaling law $P_{TH} \propto (E_p)^3$ corresponding to perturbative THG free of saturation.

source of difficulty for systematic studies of the third-harmonic intensity as a function of the temperature of the solution. At the same time, the sensitivity of the third harmonic to these variations in the linear and nonlinear-optical parameters offers a convenient way to visualize particle flows in J-aggregating solutions and image microcrystals of J-aggregates using third-harmonic generation. Broad-beam THG, in particular, points to the existence of microcrystals and agglomerates of J-aggregates in heated solutions of ethyl thiacarbocyanine [33]. The physical sizes of these structures considerably exceed the coherent sizes of J-aggregates. Optical methods, however, do not allow the structure and the type of bonds in microcrystals and agglomerates to be determined.

Experimental studies reveal correlations between the intensity of the third harmonic and two-photon-excited photoluminescence induced by femtosecond pulses of Cr:forsterite laser radiation (Fig. 11). In particular, growing pump intensity simultaneously increased the third-harmonic and photoluminescence signals. This correlation indicates the importance of effects related to population dynamics in two-photon-resonant THG in J-aggregating solutions of ethyl thiacarbocyanine and demonstrates the selective excitation of J-aggregating molecules with femtosecond pump pulses through a two-photon transition. The role of population dynamics is also sustained by the experimentally examined saturation of the third-harmonic intensity measured as a function of the pump energy (see the inset to Fig. 11). The correlation of THG and two-photon-excited photoluminescence as well as saturation of THG at high pump energies point to the probable coherent controlling of the THG process by varying the relative contributions or the relative phases of THG processes from the ground and excited states of J-aggregating molecules. An important and in many respects remarkable property of the temperature dependence of the third-harmonic intensity measured in our experiments is the correlation between third-harmonic variations and transformations of the absorption spectrum for the aggregating solution.

In contrast to absorption spectroscopy which provides the information on the structure and properties of J-aggregates averaged over the optical path of the pump beam, the third-harmonic signal can monitor J-aggregates in a small volume with the longitudinal size determined by the confocal parameter of the pump beam (see Fig. 9). Correlations between changes in the absorption spectrum of a J-aggregating solution and the intensity of the third harmonic, observed in THG experiments, suggest that the THG process is ideally suited as a local probe for J-aggregating solutions highly sensitive to the structure and sizes of J-aggregates.

The experimental results presented in this section demonstrate that THG enhanced by two-photon resonance permits us to reach a high level of nonlinear signal from the bulk of solution of J-aggregating ethyl thiacarbocyanine molecules. Third-harmonic generation in this regime is free of one-photon absorption of pump and third-harmonic radiation,

which provides favorable conditions for efficient THG and allows the generation of a spatially resolved nonlinear-optical signal from the bulk of a nonlinear medium. The femtosecond regime of optical excitation allows a high intensity of pump radiation to be reached with a minimal risk of laser-induced breakdown, leading to the generation of the nonlinear signal with an efficiency sufficient for the visualization of the aggregation process. Experimental studies reveal correlations between the intensity of the third harmonic and two-photon-excited photoluminescence induced by femtosecond pump pulses. This correlation points to the importance of effects related to population dynamics in two-photon-resonant THG in J-aggregating solutions of ethyl thiacarbocyanine and demonstrates the selective excitation of J-aggregating molecules with femtosecond pump pulses through a two-photon transition. The third-harmonic intensity has been studied as a function of the temperature of the solution. Correlations between changes in the absorption spectrum of a J-aggregating solution and the intensity of the third harmonic, revealed in these experiments, suggest that the THG process is ideally suited as a local probe for J-aggregating solutions highly sensitive to the structure and size of J-aggregates. We have thus shown that third-harmonic generation enhanced by two-photon resonances offers much promise as an efficient technique for the metrology of three-dimensional samples of optical materials based on J-aggregates and intended for photonic applications, optical data processing and transmission, and laser physics.

4. Generation of optical harmonics by carbon nanotubes

In this section, we will discuss the results of experiments devoted to the generation of the second and third harmonics by femtosecond pulses of a Cr:forsterite laser interacting with a system of single-wall carbon nanotubes (CNTs) produced by low-velocity spraying. The harmonic amplitude in these experiments obeys the power law $(I_p)^n$, being a function of the pump intensity I_p, with $n = 2$ and 3 for the second and third harmonics, respectively. This scaling law holds up to the pump intensities on the order of 10^{12} W cm^{-2}. The second and third harmonics produced by a linearly polarized pump field are also linearly polarized, with their polarization vectors oriented along the polarization direction of the pump field. The capabilities of nonlinear-optical methods for structural and morphological analysis of carbon nanotubes are taken up, and the ways to design solid-state CNT generators of optical harmonics are highlighted.

4.1 Nonlinear-optical response of carbon nanotubes

The nonlinear optics of carbon nanotubes is a new growing field of research that integrates advances in solid-state physics, laser science, photonics, the physics of low-dimensional structures, nanoscale optics, and nanotechnologies. Research activity in this field is strongly stimulated and motivated by the rapid progress in CNT technologies, opening methods of creating new materials with unique properties, including an ultrahigh strength and broadly tunable electrical conduction [21 – 24]. Theoretical studies predict strong optical nonlinearities of CNTs [113 – 116], suggesting the possibility of employing these nanoscale systems for the generation of optical harmonics, and high-order harmonics among them [117, 118]. Results of experiments devoted to the investigation of nonlinear-optical phenomena in CNT systems and to the analysis of nonlinear-optical properties of CNTs are briefly summarized in Table 2. Until recently, experimental efforts were mainly focused on optical limiting in CNT suspensions and CNT – polymer composite materials [119 – 124]. Experiments on degenerate four-wave mixing [125, 126] testify that CNTs offer much promise for the creation of new nonlinear-optical materials and the development of switching and limiting photonic devices. Experiments performed in the past few years have demonstrated the high potential of CNTs as a nonlinear material for ultrafast optics and photonics (see Table 2). Investigation of the optical Kerr effect on the femtosecond time scale in CNT solutions [127] has revealed strong fast-response optical nonlinearities in CNTs. Chen et al. [128] have shown up ultrafast optical switching in CNT – polymer composite materials. Third-harmonic generation (THG) was observed in the reflection of femtosecond Cr:forsterite-laser pulses from a CNT sample in works [29, 47, 48]. The results produced by Akimov et al. [29] suggest new possibilities of structural and topological analysis of CNTs using optical harmonic generation.

4.2 Interaction of laser radiation with carbon nanotubes

The quasi-one-dimensional structure of carbon nanotubes opens a clue to understanding the regimes of interaction of laser radiation with CNT ensembles [129 – 131]. Quantum

Table 2. Nonlinear-optical phenomena experimentally established in CNT materials.

Process	Nonlinear susceptibility	CNT samples	Laser	Laser pulse duration	References
Optical limiting	$\chi^{(3)}(\omega;\omega,-\omega,\omega)$	Suspensions and polymer composites	mostly Nd:YAG laser	nano- and picosecond pulses	[119 – 124]
Degenerate four-wave mixing	$\chi^{(3)}(\omega;\omega,-\omega,\omega)$	Suspension	Nd:YAG laser	8 ns, 30 ps	[125]
		Solid-state sample	Nd:YAG laser	nanosecond pulses	[126]
Optical Kerr effect	$\chi^{(3)}(\omega;\omega,-\omega,\omega)$	Solution	Ti:sapphire laser	120 fs	[127]
Optical switching	$\chi^{(3)}(\omega;\omega,-\omega,\omega)$, $\chi^{(3)}(\omega_2;\omega_2,-\omega_1,\omega_1)$	Polymer composites	Fiber laser	150 fs	[128]
Third-harmonic generation	$\chi^{(3)}(3\omega;\omega,\omega,\omega)$	Solid-state sample	Cr:forsterite laser	160 fs	[47]
				75 fs	[29, 48]
Second-harmonic generation	$\chi^{(2)}(2\omega;\omega,\omega)$	Solid-state sample	Cr:forsterite laser	75 fs	[29, 48]

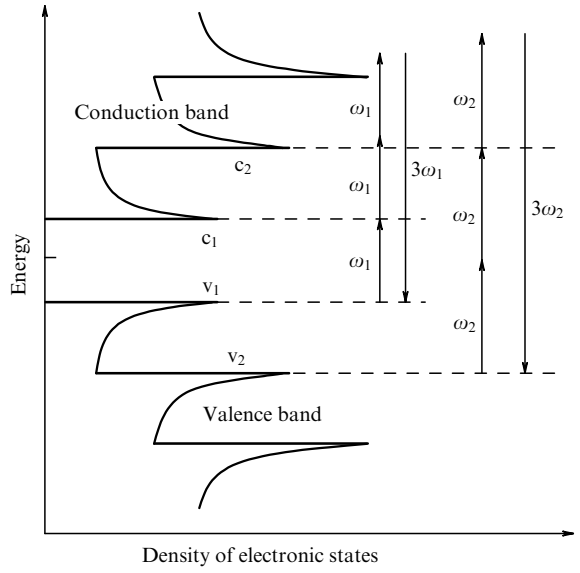

Figure 12. Spectral diagram of the density of electronic states for a carbon nanotube, featuring van Hove singularities. Third-harmonic generation can be enhanced in a system of carbon nanotubes due to one- and two-photon resonances at the frequencies of the first ($v_1 \rightarrow c_1$) and second ($v_2 \rightarrow c_2$) optical van Hove transitions between the states in the valence and conduction bands.

confinement of electron motion in the directions perpendicular to the nanotube axis is manifested in the density spectrum of electronic states [132], which displays van Hove singularities (Fig. 12). Fluorescence and Raman studies [133, 134] evidence a strongly resonant character in the interaction of laser radiation with CNTs, revealing the significance of optical van Hove transitions between electronic states in the valence and conduction bands (see Fig. 12).

The use of strong optical nonlinearities of CNT systems for the generation of reliably detectable harmonic signals, resulting from the nonlinear coherent scattering of pump radiation from CNTs and carrying the information on the structure and physical properties of CNTs, is at the heart of our harmonic-generation experiments described in this section. Optical harmonics were generated in our experiments using pump radiation with a wavelength of 1.25–1.27 μm, produced by a femtosecond Cr:forsterite laser. Within this wavelength range, the scattering of radiation by CNT systems can be enhanced due to a series of one-photon resonances corresponding to $v_1 \rightarrow c_1$ transitions between the electronic states in the valence and conduction bands (see Fig. 12) with CNT indices (10, 3), (10, 5), (11, 1), (8, 7), (13, 2), and (9, 5), as well as two-photon resonances corresponding to $v_2 \rightarrow c_2$ transitions (see Fig. 12) with CNT indices (10, 3), (7, 5), (11, 1), and others.

Absorption spectra of CNT samples employed in experiments by Akimov et al. [29, 48] display clearly resolved peaks at 1.28 and 2.2 eV. These peaks are attributed to optical van Hove transitions. Pump radiation used in our experiments is thus red-detuned from both one- and two-photon resonances with the frequency of optical transitions characteristic of the predominant type of CNTs in the samples. However, the optical density of our CNT systems at an energy of 2 eV, corresponding to the exact two-photon resonance under the experimental conditions, is only a few percent lower than the optical density at the maximum of the absorption band. The samples investigated are, therefore, characterized by a sufficiently high content of CNTs with the spectra of electronic states meeting conditions of a two-photon resonance with the frequency of a Cr:forsterite laser.

The efficiency of nonlinear-optical processes, including second-harmonic generation (SHG) and THG, increases with the growth in the pump radiation intensity. Laser-induced breakdown, however, imposes a limitation on the pump intensity. In the case of shorter pulses, the efficiency of nonlinear-optical interactions in solids can often be increased due to higher intensities corresponding to laser fluences at the threshold of optical breakdown. To illustrate this possibility, we invoke the following qualitative arguments.

Let us represent the intensities of the second and third harmonics, I_{SH} and I_{TH}, perturbatively generated by a pump pulse with an intensity right below the breakdown threshold as

$$I_{SH} \propto \left|\chi^{(2)}\right|^2 \left[\frac{F_{th}(\tau)}{\tau}\right]^2, \qquad I_{TH} \propto \left|\chi^{(3)}\right|^2 \left[\frac{F_{th}(\tau)}{\tau}\right]^3,$$

where $\chi^{(n)}$ is the nth-order nonlinear-optical susceptibility, $n = 2, 3$; $F_{th}(\tau)$ is the breakdown threshold fluence, and τ is the pump pulse duration. With the scaling law $F_{th} \propto \tau^{1/2}$, which is typical of a broad class of optical materials irradiated with pulses having durations $\tau > 10$ ps [135–137], the intensities of the second and third harmonics scale as $I_{SH} \propto 1/\tau$ for SHG, and $I_{TH} \propto 1/\tau^{3/2}$ for THG. For shorter laser pulses, including pulses in the femtosecond range of durations, the dependence of the threshold fluence on the pulse duration becomes even slower than $F_{th} \propto \tau^{1/2}$ [136], allowing even higher intensities of the second and third harmonics to be achieved around the breakdown threshold [27]. The employment of femtosecond pulses in our experiments thus results in a substantial increase in the yield of optical harmonics as compared with the picosecond regime. This argument agrees well with the results of earlier experiments on four-wave mixing in CNTs [126], performed with the use of nanosecond pump pulses.

4.3 Optical-harmonic generation and structural analysis of carbon nanotubes

In experiments [29, 48], femtosecond pulses of a Cr:forsterite laser were utilized to study second- and third-harmonic generation in CNT samples produced by low-velocity spraying [129, 130]. One of the main advantages of this technique is that carbon nanoparticles produced by laser-induced pyrolysis at the first stage of this process are then used as a solid precursor for CNT growth with no metal catalysts which are usually employed in standard CNT technologies [131, 132]. No additional purification is therefore required for CNT samples produced with the adoption of this technique. The morphology and the composition of CNT samples were analyzed with scanning electron microscopy and Raman scattering spectroscopy. The diameter of CNTs in the samples under study ranged from 0.9 up to 1.5 nm. The CNT length exceeded 1 μm. Analysis of scanning electron microscope images [29] shows that CNTs tend to form bundles in the studied samples with a typical diameter of about 30 nm.

Harmonic signals were detected in transmission geometry. Spectral and polarization properties of optical harmonics were investigated, and the harmonic yields were measured as functions of the pump radiation intensity. The second- and

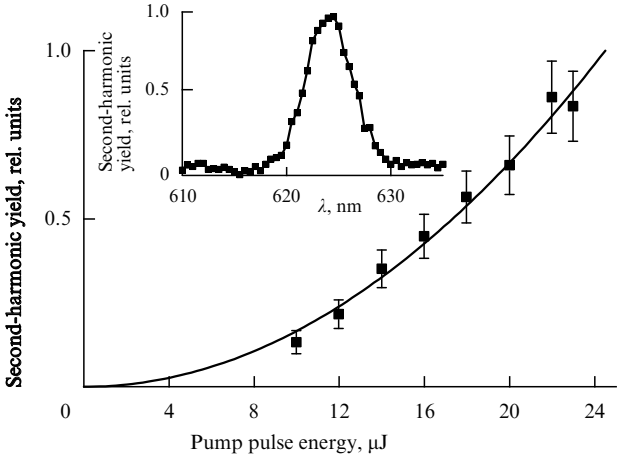

Figure 13. The yield of the second harmonic generated by a CNT system as a function of the energy of a 75-fs Cr:forsterite-laser pump pulse. The diameter of the focused pump beam on the surface of the CNT sample is 120 μm. The solid line represents the quadratic fit. The inset shows the spectrum of the second harmonic.

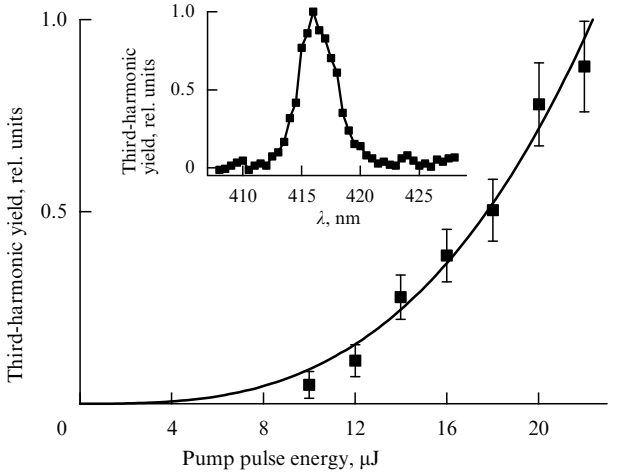

Figure 14. The yield of the third harmonic generated by a CNT system as a function of the energy of a 75-fs Cr:forsterite-laser pump pulse. The diameter of the focused pump beam on the surface of the CNT sample is 120 μm. The solid line represents the cubic fit. The inset shows the spectrum of the third harmonic.

third-harmonic yields scaled as $(I_p)^n$ (see Figs 13, 14), where I_p is the pump intensity, and n is the harmonic number, within the range of pump intensities up to at least 10^{12} W cm^{-2}, indicating the perturbative regime of nonlinear-optical interactions. The intensity of the nth harmonic in this regime is given by the expression

$$I_n \propto \left|\chi^{(n)}\right|^2 I_p^n ,$$

where $\chi^{(n)}$ is the nth-order nonlinear-optical susceptibility. The experimental data thus evidence that the nonlinear-optical susceptibilities $\chi^{(n)}$ ($n = 2, 3$) are independent of the pump intensity. The results of these measurements demonstrate that the intensity range of unsaturated growth of the harmonic yield can be extended under certain conditions up to 10^{12} W cm^{-2}.

The spectra of the second and third harmonics generated by femtosecond pulses of a Cr:forsterite laser, passing through a CNT sample, are depicted in the insets to Figs 13 and 14, respectively. Importantly, the ratio η of the harmonic signal at the center of harmonic spectral lines to the background is 30 for third-harmonic generation, and 50 for second-harmonic generation under conditions of our experiments, suggesting THG and SHG as sensitive techniques for CNT detection in transparent materials. The second and third harmonics produced by a linearly polarized pump field were also linearly polarized, with their polarization vectors oriented along the polarization direction of the pump field. The fact that linearly polarized pump radiation gives rise to linearly polarized second and third harmonics with a very low depolarization degree opens the path to analyzing the structure properties of CNTs through polarization measurements on the second and third harmonics.

In view of an amazing diversity of carbon nanotubes featuring different point-group symmetries and broadly tunable, structure-sensitive band gaps [138], nonlinear-optical techniques offer much promise as a tool for local probing of CNTs, which is capable of detecting the band gap and identifying the spatial structure of nanotubes. In particular, second-harmonic generation is governed by the second-order nonlinear susceptibility $\chi^{(2)}(2\omega;\omega,\omega)$ which vanishes for centrosymmetric media. Second-harmonic generation thus allows the detection of nanotubes in a host made of centrosymmetric material with no background related to the nonlinearity of the host. The second harmonic can be generated in CNT materials through surface nonlinear-optical interactions, as well as due to nondipole nonlinear terms or the chirality of some types of CNTs. Methods of measurements distinguishing between these SHG mechanisms would allow second-harmonic generation to be used for identifying the type of CNTs and detecting chiral nanotubes in a sample. Ensembles of chiral CNTs are of special interest for practical implementation of concepts related to the nonlinear optics of media with broken mirror symmetry and for observation of a new class of nonlinear-optical phenomena inherent in chiral materials [4, 139 – 142].

Experimental studies intimate that quasi-one-dimensional CNT structures offer new possibilities for optical harmonic generation. Quantum confinement gives rise to singularities in the density spectrum of electronic states. Such systems possess strong nonlinearities which can be enhanced due to one- or multiphoton resonances (see Fig. 12), opening up new avenues for developing solid-state generators of high-order optical harmonics. An illuminating and comprehensive overview of the role of one- and multiphoton resonances in optical-harmonic generation is provided in classical textbooks on nonlinear optics [56, 107]. The frequencies of optical van Hove transitions are determined by the CNT diameter d and the chiral angle α. In particular, the frequencies v_i of the first ($i = 1$) and second ($i = 2$) van Hove transitions $v_1 \rightarrow c_1$ and $v_2 \rightarrow c_2$ (see Fig. 12) are approximated by the following expression [133, 134]: $v_i = a/(b + c_i d) + A_{nm}\cos(3\alpha)/d^2$, where a is a constant, b_i and c_i are the parameters varying for different optical transitions, and A_{nm} is the parameter depending on the CNT indices m and n. Methods of nonlinear spectroscopy can thus be employed for probing the structure and determining the sizes of carbon nanotubes.

Table 2 gives the experimental results presented in this section in the context of earlier studies on the nonlinear optics

of CNTs, highlighting several important aspects of optical-harmonic generation in CNT systems, which were revealed by recent work. Amplified 75-fs pulses of a Cr:forsterite laser can efficiently generate reliably detectable second and third harmonics in a system of single-wall CNTs. Under these conditions, the second- and third-harmonic yields scale as $(I_p)^n$, where I_p is the pump intensity, and n is the harmonic number, within the range of pump intensities up to 10^{12} W cm^{-2}. High-contrast second-, third-, and fifth-harmonic signals detected in CNT experiments suggest that optical harmonics can be considered as a highly sensitive probe for the diagnostics of carbon nanotubes.

5. Femtosecond nonlinear-optical metrology of nanocomposite materials

In this section, we will show that optical-harmonic generation by femtosecond laser pulses can be used for nonlinear-optical metrology of nanocrystal assemblies and nanopowder materials. We will discuss the results of experiments that demonstrate the capability of femtosecond second- and third-harmonic generation to probe the structure and the spatial symmetry of nonlinear-optical nanocrystals embedded in transparent hosts. A drastic enhancement of SHG efficiency, observed when decreasing the wavelength of femtosecond pump pulses, indicates an important contribution of scattering effects to nonlinear-optical interactions in nanopowder materials.

5.1 Methods of nonlinear optics and nanocomposite materials

Nonlinear-optical methods can provide much important information on the composition, structure, and spatial symmetry of materials [56, 143, 144]. Nonlinear-optical techniques are ideally suited for the on-line monitoring of phase transitions and crystal-lattice dynamics [145, 146], as well as for probing ultrafast electron dynamics in assemblies of metal nanoparticles [147]. Recent studies have demonstrated the utility of second-harmonic generation for microscopy of single micrometer-sized particles on a substrate [148] and probing the surfaces of submicron particles [149, 150]. Optical-harmonic generation and four-wave mixing processes also open up fresh opportunities for nonlinear microscopy. In particular, third-harmonic generation proved to be a very useful tool for a microscopy of biological objects [110, 111] and laser-produced plasmas [34, 112]. Coherent anti-Stokes Raman scattering (CARS) constitutes another four-wave mixing technique that offers much promise for microscopic applications [151 – 153], extending the ideas of spontaneous Raman microscopy [154, 155] to the coherent domain and providing important advantages related to the coherent nature of the CARS signal. Nanoscale systems and nanocomposite materials make up new objects of nonlinear optics. Nonlinear-optical methods can be employed with advantage to gather unique information about assemblies of nanocrystals in nanocomposite systems. Nanopowder materials in due course can be utilized for nonlinear-optical spectral transformations of ultrashort pulses, offering new solutions for ultrafast optics and photonics.

Recent experiments [27, 28, 32, 156] have demonstrated the potential of second- and third-harmonic generation for the analysis of the properties and metrology of silicon carbide (SiC) nanocrystals embedded in thin polymethyl methacrylate (PMMA) films. Due to a rather wide band gap, high hardness, high chemical stability, and high resistance to corrosion and high temperatures, silicon carbide is considered as a promising technological material [157 – 166], in particular, as an excellent candidate for the creation of microsensors and microsystems intended for operating under extreme conditions and in harsh environments.

Silicon carbide is an interesting object for nonlinear optics. Due to its strong optical nonlinearities [167 – 170] and pronounced polytypism, SiC could allow creation of new nonlinear-optical materials. Methods of nonlinear optics, on the other hand, can provide new information not only on the composition of SiC-containing materials, but also on the polytype of SiC nanocrystals.

5.2 Properties of the second and third harmonics

In experiments [27, 28, 32], amplified femtosecond pulses of a Cr:forsterite laser were applied to study the properties of the second and third harmonics generated in PMMA films doped with silicon carbide nanocrystals. The procedure employed to produce nanocomposite films for these experiments included two stages [27, 31]. At the first stage, silicon carbide nanoparticles with controlled sizes were produced through a dissociation of silane (SiH_4) and acetylene molecules under the action of continuous-wave CO_2-laser radiation with a wavelength of 10.6 μm and a power of 1.5 kW. At the second stage, the preparation strategy included dispersing SiC nanoparticles into methyl methacrylate monomer. This mixture was then polymerized in several stages at a high temperature. Nanocomposite films produced by this technique had a thickness of 50 – 200 μm. The sizes of SiC nanocrystals in these films typically ranged from 10 to 80 nm. Typical surface scanning electron microscope (SEM) images of SiC nanopowder polymer films are presented in Fig. 15. Luminescent spectroscopy studies [27] indicate the predominance of the 6H-SiC polytype in the samples prepared.

The second-harmonic signal was observed as a bright red spot on an SiC nanopowder film, visible with the naked eye [27, 28, 31, 32]. The efficiency of THG was much lower. The intensities of the second and third harmonics scaled in these experiments as the second and third powers of the pump pulse energy within the entire studied range of laser intensities up to the breakdown threshold (Figs 16, 17). Deviations from these scaling laws were observed only under conditions of optical breakdown, accompanied by irreversible changes in the structure of samples. These findings point to a purely perturbative regime of optical-harmonic generation in the studied nanocomposite samples with field-independent nonlinear-optical susceptibilities. In practical terms, the observed scaling power laws are especially convenient for metrological purposes, as they allow a very simple normalization of harmonic signals to the pump power.

Since SHG is allowed in the dipole approximation only in noncentrosymmetric media, this nonlinear process permits background-free visualization of nanocrystal assemblies embedded in a substrate or a film made of a centrosymmetric material. Nanocomposite SiC/PMMA films studied in experiments [27, 28, 32] belong specifically to this class of objects. Second-harmonic generation by noncentrosymmetric SiC nanocrystals is controlled by the second-order polarization $P_i(2\omega) \propto \chi^{(2)}_{ijk}(2\omega;\omega,\omega)\,E_jE_k$, where $\chi^{(2)}_{ijk}(2\omega;\omega,\omega)$ is the second-order nonlinear-optical susceptibility of the medium responsible for SHG, while E_j and E_k are the electric-field

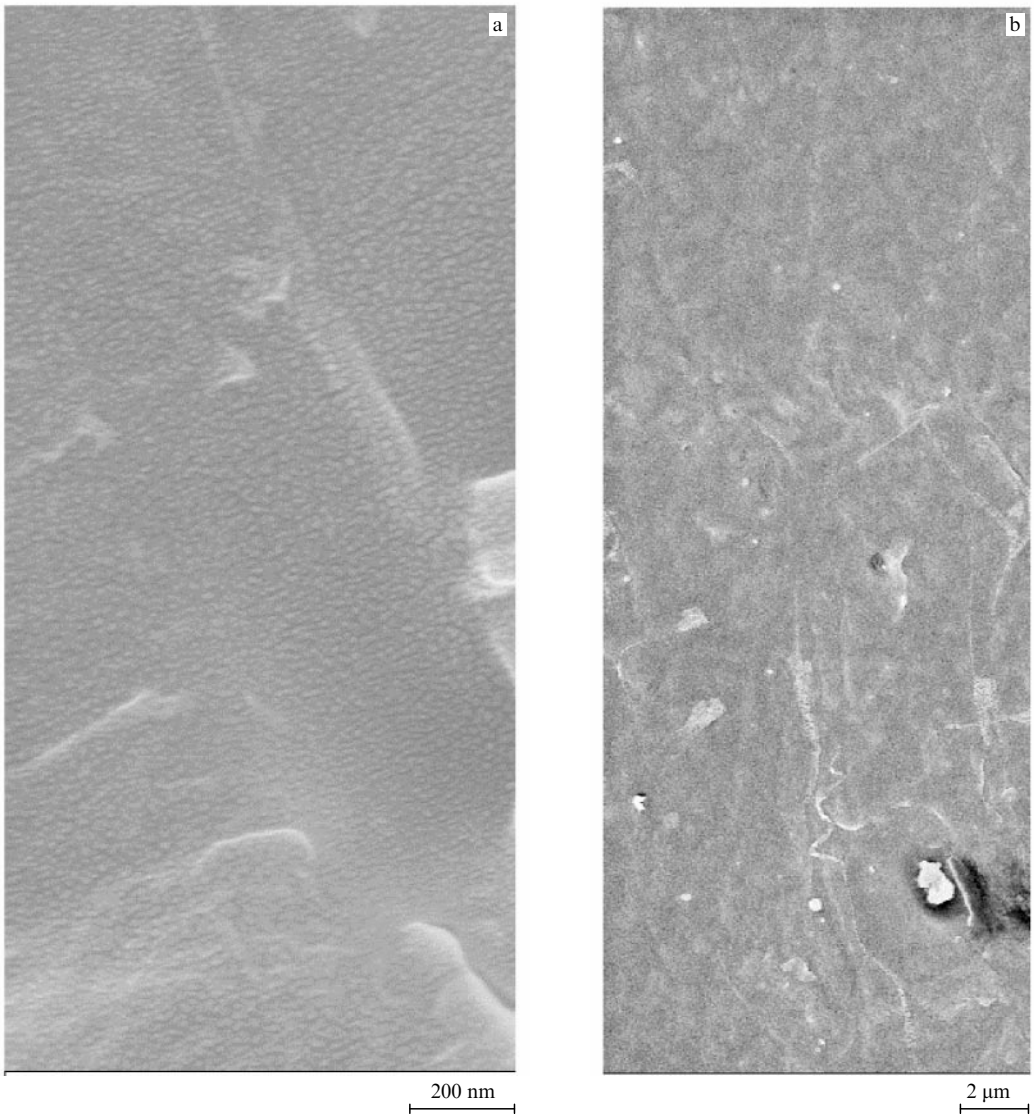

Figure 15. Surface scanning electron microscope images of polymer films doped with SiC nanocrystals. The markers below the images correspond to spatial scales of (a) 200 nm, and (b) 2 μm.

vector components of the pump. The tensor properties of the SHG nonlinear susceptibility $\chi^{(2)}_{ijk}(2\omega;\omega,\omega)$ are dictated by the point-group symmetry of SiC nanocrystals. Hexagonal SiC polytypes display the 6*mm* point-group symmetry and have three independent nonvanishing components of SHG susceptibility: $\chi^{(2)}_{zzz}$, $\chi^{(2)}_{zxx}$, and $\chi^{(2)}_{xzx}$, with the z-axis chosen along the sixfold-symmetry axis [169]. The condition $\chi^{(2)}_{xzx} = \chi^{(2)}_{xxz}$ always holds true for SHG, since the last two indices can be permuted as long as the frequency arguments are the same. In the static limit, the Kleinman relations $\chi^{(2)}_{zxx}(0) = \chi^{(2)}_{xzx}(0)$ leave only two independent components in the SHG second-order susceptibility tensor. Theoretical analysis predicts the following ratio of static limit $\chi^{(2)}_{ijk}(2\omega;\omega,\omega)$ components for 6H-SiC polytypes: $|\chi^{(2)}_{zzz}/\chi^{(2)}_{xzx}| \approx 1.8$ [169, 170]. Experiments by Niedermeier et al. [171], on the other hand, give $|\chi^{(2)}_{zzz}/\chi^{(2)}_{xzx}| \approx 6$. Silicon carbide nanocrystals with optical axes randomly oriented in the polymer film (see the inset to Fig. 16) thus give rise to a depolarized second harmonic (inset to Fig. 18). This depolarization is enhanced by scattering. The influence of scattering effects will be discussed in greater detail in the following section.

5.3 Nanostructured materials for femtosecond technologies

Nanostructured materials open new unique opportunities in laser physics, photonics, and optical technologies. Nanopowder materials, in particular, are at the heart of lasers of a new architecture [172–174]. Nano- and mesoporous semiconducting materials can radically enhance nonlinear-optical frequency conversion of laser radiation [175–177]. Photonic-crystal structures are intensely used for controling radiative processes and are considered as promising candidates for the creation of a new generation of components and devices for telecommunications, laser physics, and nonlinear optics [3]. Microstructured and photonic-crystal fibers [62–64] provide unprecedentedly high efficiencies of supercontinuum generation [3, 77] and nonlinear-optical spectral transformation of low-energy ultrashort laser pulses [68, 77]. Optical fibers of this type are widely employed in optical metrology [178, 179], nonlinear optics of ultrashort pulses [180], optical coherence tomography [181], photochemistry [182], and spectroscopy [39, 183].

In this section, we explore possibilities of enhancing the frequency conversion of ultrashort pulses in polymer films

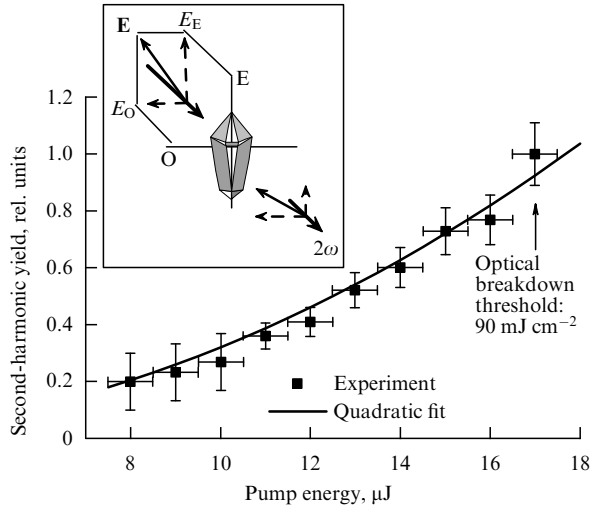

Figure 16. The yield of the second harmonic generated in a polymer film doped with SiC nanocrystals as a function of the pump pulse energy. The duration of the pump pulse is 75 fs. The diameter of the pump beam focused on the sample is 120 μm. The solid line represents the quadratic fit. The inset shows a diagram of second-harmonic generation by a randomly oriented silicon-carbide nanocrystal.

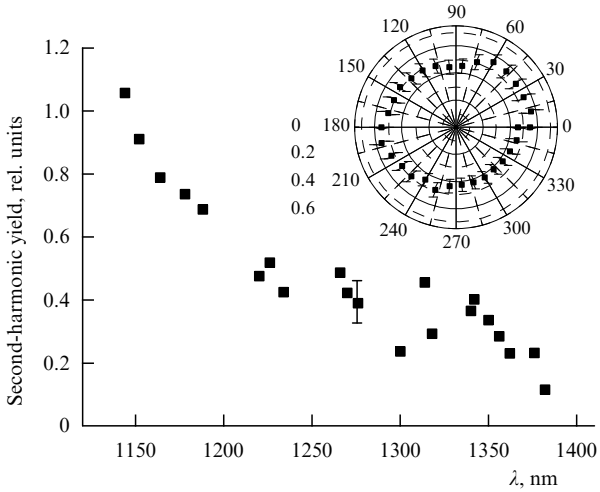

Figure 18. The yield of the second harmonic generated in reflection from a 100-μm-thick polymer film doped with SiC nanocrystals with a mean size of about 50 nm as a function of the pump radiation wavelength. The second-harmonic signal is normalized to include the frequency responses of the photomultiplier and the monochromator. The inset shows the polarization dependence of the efficiency of SHG by a linearly polarized pump field. The polarization vector of the pump field is oriented at 15° on this polar plot.

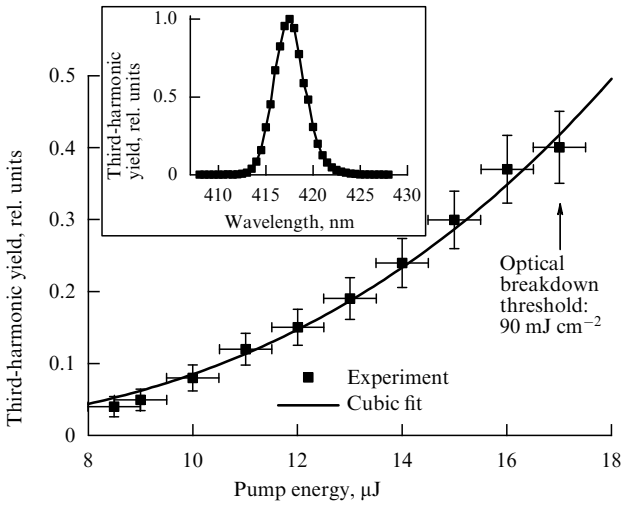

Figure 17. The yield of the third harmonic generated in a polymer film doped with SiC nanocrystals as a function of the pump pulse energy. The duration of the pump pulse measures 75 fs. The diameter of the pump beam focused on the sample is 120 μm. The solid line represents the cubic fit. The inset shows the spectrum of the third harmonic.

doped with nanopowders of nonlinear-optical materials. Nonlinear-optical processes in powder materials have been studied earlier in the context of several interesting fundamental problems and various applications [184]. Second-harmonic generation in microcrystallites of materials with a high second-order nonlinearity, advanced by Kurtz and Perry [185] as a method for coherence-length assessment, is a classical example of a nonlinear-optical process in a powder system. The approach to SHG proposed in works [27, 28, 32] is based on the use of thin polymer films doped with nanopowders of materials with a quadratic nonlinearity. Silicon carbide was employed as a nonlinear material in this strategy. The second-order optical nonlinearity of silicon carbide has been investigated earlier in Refs [167–171]. The size of nanocrystals in nanopowder polymer films used in experiments [27, 28, 32] ranged from 10 up to 80 nm. Experimental results [156] presented below in this section reveal a substantial contribution of scattering effects to nonlinear-optical interactions in nanopowder materials, suggesting strategies for a radical enhancement of SHG by optimizing the relation between the film thickness and the elastic-scattering length of photons in nanopowder materials.

The second harmonic is generated in the studied nanopowder films due to the second-order optical nonlinearity of silicon carbide nanocrystals. The second harmonic of incident radiation from an optical parametric amplifier was observed both in reflected and in transmitted light. Figure 18 displays the second-harmonic yield in reflection from a polymer film with a thickness of about 100 μm and an average size of SiC nanocrystals of about 50 nm as a function of the pump radiation wavelength. As can be seen from the results presented in Fig. 18, the SHG efficiency in a system of randomly oriented SiC nanocrystals in a nanopowder film increases with a decrease in the pump wavelength. This effect reveals the significance of light scattering in nonlinear-optical interactions of laser pulses in random media, including nonlinear nanopowder materials.

To quantify the role of scattering effects in SiC nanopowder films, we estimate the elastic scattering length for photons propagating through a random medium. The theory of Rayleigh scattering for a system of spherical scatterers with a radius a and a dielectric constant ε_1, randomly distributed in a material with a dielectric constant ε_2, yields the following expression for the length l of elastic scattering of radiation with the wavelength λ [186]:

$$l = 9(2f)^{-1}\left(\frac{\lambda}{2\pi}\right)^4 a^{-3}(\varepsilon_1 - \varepsilon_2)^{-2},$$

where f is the volume filling factor (volume fraction) of scattering nanoparticles.

The elastic scattering length for the photons of pump radiation with a wavelength of 1.35 μm in a PMMA film doped with SiC nanopowder is estimated as $l \sim 150$ μm, which exceeds the film thickness. For a pump wavelength of 1.15 μm, however, the elastic scattering length, $l \sim 80$ μm, becomes less than the film thickness. Thus, tuning the pump wavelength within the range of 1.15 – 1.35 μm, we qualitatively change the relation between the elastic scattering length of pump photons and the thickness of the nanopowder film. The radical enhancement of SHG, revealed in experiments for shorter pump wavelengths, indicates the significant influence of scattering effects on nonlinear-optical processes in nanopowder materials. The efficiency of light scattering increases as the wavelength of pump radiation becomes shorter. Scattering processes broaden the angular spectrum of wave vectors of pump photons, facilitating the phase matching of pump and second-harmonic fields in a system of randomly oriented SiC nanocrystals.

The radical enhancement of SHG observed in experiments suggests the general strategy for improving the efficiency of nonlinear-optical processes in nanopowder materials, offering recipes for the creation of cost-efficient and compact frequency converters for ultrashort laser pulses, which are based on polymer films doped with nanocrystals of materials with a high optical nonlinearity.

6. Femtosecond biophotonics

Laser biomedicine is one of the most important and rapidly growing areas of interdisciplinary applied laser research. Since the light employed to visualize the microstructure of biological tissues in an optical biopsy is subject to attenuation due to absorption and scattering, much attention is currently focused on searching for optimal sources of light that would ensure the maximum penetration depth and would possess sufficient power to ensure reliable signal detection in various modes used to image biological systems. While absorption of human tissues (mainly due to water and melanin) is relatively weak within the so-called therapeutic window [187], attenuation due to the light scattering makes light sources within the range of wavelengths from 1.2 to 1.3 μm especially suitable for the purposes of medical diagnostics. Recently, superluminescent diodes (SLDs) with emission wavelengths lying in the range from 850 to 1300 nm have gained wide acceptance [188 – 192] as convenient sources for optical coherence tomography (OCT) [193]. Intrinsic problems of SLD-based optical systems stem from the limited optical power characteristic of these sources (typically, in the milliwatt range). In particular, it is difficult to expect that the use of SLDs may ensure a sufficient efficiency of nonlinear-optical methods of optical imaging and microscopy, which have been recently demonstrated for different biological objects. On the other hand, Ti:sapphire lasers, capable of ensuring high radiation powers, excellent time resolution, and a high resolution of OCT imaging, cannot provide sufficient radiation penetration depths in biological tissues [194].

All these factors make femtosecond Cr^{4+}:forsterite lasers an attractive source for a broad range of medical applications. Due to the longer wavelength, the scattering cross section of Cr^{4+}:forsterite-laser radiation in biological tissues is much less than that typical of Ti:sapphire lasers, while absorption of biological tissues is reasonably low within the wavelength range covered by Cr^{4+}:forsterite lasers. All-solid-state Cr:forsterite lasers have recently been shown to be an optimal choice for high-signal-to-noise-ratio OCT imaging, allowing a resolution of several microns to be achieved [35, 195]. An up-to-date review of femtosecond Cr:forsterite lasers for biological studies and medical applications can be found in Refs [37, 196].

Due to the short pulse duration, a relatively high power of laser pulses, and chirp tunability, Cr:forsterite lasers offer much promise for optical coherence tomography, as well as nonlinear-optical imaging and microscopy of biological samples and organic molecules, including microscopy based on second- and third-harmonic generation [110, 111, 197 – 200]. As demonstrated by Squier et al. [110, 200], 18 mW of 1.2-μm 100-fs radiation is sufficient to perform dynamic imaging of living objects with the use of THG microscopy. Optical parametric amplifiers were used to perform THG microscopic measurements in Refs [198, 199]. The pulse energy and the pulse duration attainable with the Cr:forsterite laser described in this paper give grounds to believe that such a source may be extremely useful, allowing high efficiencies of THG and high temporal resolution to be achieved in the scheme of dynamic THG microscopy. The high pulse energy, a short pulse duration, and a large penetration depth of femtosecond Cr:forsterite-laser pulses are also favorable for the time-gating imaging technique involving second-harmonic generation, earlier implemented by Kuditcher et al. [201] with a Ti:sapphire laser.

The level of the pulse power provided by Cr:forsterite lasers with regenerative amplification is sufficient for many biological and medical applications. Thus, laser systems of this class are ideally suited in their power, temporal, and spectral parameters for high-resolution optical coherence tomography applications and nonlinear-optical tissue imaging. The intra- and extracavity chirp control of Cr:forsterite-laser pulses [202] allows OCT imaging with tunable resolution depth to be implemented.

Another promising trend in femtosecond biophotonics involves an application of quantum control for steering vibrational wave-packet dynamics in molecular systems. One of the goals of this activity is to develop optically switched biomaterials and biophotonic devices. Photochromic compounds [203 – 207] constitute promising candidates that can help to solve this problem. The photochromism in spiropyran compounds, for example, proceeds through C – O bond cleavage in an initially nonexcited molecule (form A in Fig. 19) and relaxation from a transient state (state X in Fig. 19) to a metastable merocyanine-form state (state B). Time-resolved studies performed with the use of femtosecond pulses [208 – 210] have revealed the existence of an initial fast phase of this photochromic reaction, occurring on a subpicosecond time scale. Experimental investigation of photochromic processes initiated by two-photon absorption of femtosecond laser pulses in a bulk polymer sample doped with spiropyran suggests the possibility of controling photochromism in the solid phase by varying the polarization state and the chirp of laser pulses [211, 212]. In particular, negatively chirped laser pulses can provide higher efficiencies of the photochromic process as compared with transform-limited or positively chirped pulses. This result can be interpreted in terms of the dynamics of vibrational wave packets excited by femtosecond laser pulses in the molecular system of spiropyran (see Fig. 19). This model represents the C – O bond cleavage as an evolution of a wave packet that consists of vibrational states in an electronically excited level of a spiropyran molecule and that arises as a result of

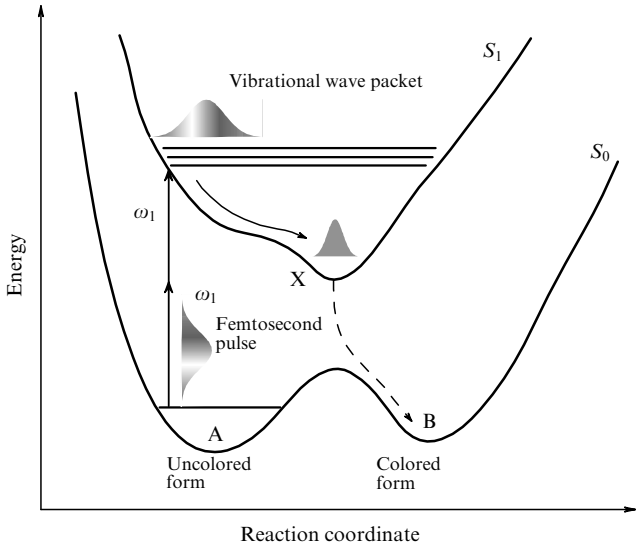

Figure 19. Quantum-controlled photochromism. Two-photon absorption of a femtosecond laser pulse with a frequency ω_1 from the ground state (S_0) of a photochromic molecule produces a wave packet consisting of vibrational states in an electronically excited term (S_1). The wave packet evolves toward the transient state X. Relaxation from this state generates photochromic molecules in metastable form B. Due to the anharmonicity of the potential sensed by the electronically excited state, the time intervals required to reach state X are different for individual vibrations forming the wave packet. Pulses with an appropriate initial chirp can focus molecular vibrations in the target state X on the potential surface.

absorption of two photons from the field of a femtosecond laser pulse. The metastable form B, as indicated by extensive experimental data [209, 210], is reached through relaxation from the transient state X, which is formed, in its turn, as a result of the evolution of the vibrational wave packet. Due to the anharmonicity of the potential sensed by the electronically excited state, the time intervals required to reach the state X are different for individual vibrations forming the wave packet. Pulses with an appropriate initial chirp, in accordance with the generic concept of quantum control with chirped pulses [213, 214], can focus molecular vibrations in the target state X on the potential surface. A more precise, quantitative analysis of wave-packet evolution is still not possible at this stage because of the lack of data on potential surface details for spiropyran molecules in a solid host. Quantum control of photochromic processes demonstrated in Refs [211, 212] paves the ways for creating coherence- and polarization-controlled components for photonics, telecommunications, and three-dimensional optical data storage, suggesting attractive strategies for the development of optically switchable biomaterials and biophotonic devices.

7. Conclusions

The material presented in this review illustrates the basic physical factors and phenomena behind interesting scenarios of interaction of ultrashort laser pulses with nanoscale objects, nanocomposite materials, supramolecular structures, and molecular aggregates. Femtosecond laser pulses offer a way to achieve high intensities of electromagnetic radiation without irreversible damage to materials, making it possible to observe unique regimes of interaction of the light field with nanostructures and molecular aggregates. Dielectric and electron confinement, as well as resonances due to quantum size effects and collective phenomena in supramolecular and aggregated structures, radically enhance nonlinear-optical interactions of ultrashort pulses. Experimental results on optical-harmonic generation in polymer films doped with silicon carbide nanocrystals, discussed in this review, illustrate the potential of dielectric confinement for the creation of new materials with a tailored optical response for nonlinear optics, laser physics, and ultrafast photonics. Effects of electron confinement are clearly manifested in nonlinear-optical phenomena observed in CNT systems. Nonlinear-optical processes enhanced by resonances which in turn are induced by collective interactions in supramolecular nanostructures provide a convenient and efficient tool for the visualization of molecular aggregation. The physical phenomena considered in this review advance new interesting solutions to the development of highly sensitive nonlinear-optical methods for the structure and morphology analysis of nanostructured materials. These effects also suggest new strategies for the control, switching, and transformation of ultrashort laser pulses.

Acknowledgments. Fruitful collaboration and illuminating discussions with S O Konorov, D A Akimov, A A Podshivalov, A N Petrov, D A Sidorov-Biryukov, A B Fedotov, P K Kashkarov, L A Golovan', and E P Grabchak are gratefully acknowledged. Material presented in this paper largely reflects the results of research carried out at the Center of Photochemistry, Russian Academy of Sciences, and the Physics Department of M V Lomonosov Moscow State University in cooperation with R Fantoni and S Botti (ENEA, Frascati, Italy); D Chorvat, D Chorvat Jr., and I Bugar (International Laser Center, Bratislava, Slovak Republic); M Avella and M E Errico (Institute of Chemistry and Technology of Polymers, Pozzuoli, Italy); V I Beloglazov and N B Skibina (Institute of Technology and Equipment for Glass Structures, Saratov); P Russell, T Birks, and W Wadsworth (University of Bath, UK), and Yu N Kondrat'ev, V S Shevandin, K V Dukel'skiĭ, and A V Khokhlov (S I Vavilov State Optical Institute, St.-Petersburg). We are cordially grateful to all our collaborators.

This study was supported in part by the President of the Russian Federation Grant MD-42.2003.02, the Russian Foundation for Basic Research (projects Nos 03-02-16929 and 02-02-17098), and INTAS (projects Nos 03-51-5037 and 03-51-5288). The research described in this publication was made possible in part by Award No. RP2-2558 from the U.S. Civilian Research & Development Foundation for the Independent States of the Former Soviet Union (CRDF). This material is also based upon work supported by the European Research Office of the US Army under Contract No. 62558-03-M-0033.

References

1. Joannopoulos J D, Meade R D, Winn J N *Photonic Crystals: Molding the Flow of Light* (Princeton, NJ: Princeton Univ. Press, 1995)
2. Sakoda K *Optical Properties of Photonic Crystals* (Berlin: Springer-Verlag, 2001)
3. Bowden C M, Zheltikov A M (Eds) "Nonlinear optics of photonic crystals: Feature issue" *J. Opt. Soc. Am. B* **19** (9) (2002)
4. Verbiest T et al. *Science* **282** 913 (1998)
5. Kobayashi T (Ed.) *J-Aggregates* (Singapore: World Scientific, 1996)
6. Prasad P N, Williams D J *Introduction to Nonlinear Optical Effects in Molecules and Polymers* (New York: Wiley, 1991)

7. Bredas J L et al. *Chem. Rev.* **94** 243 (1994)
8. Bubeck C, in *Organic Thin Films for Waveguiding Nonlinear Optics* (Adv. in Nonlinear Optics, Vol. 3, Eds F Kajzar, J D Swalen) (Amsterdam: Gordon & Breach, 1996) p. 137
9. Meier U et al. *Synthetic Met.* **109** 19 (2000)
10. Beltrani T et al. *Polymer* **42** 4025 (2001)
11. Gubler U et al. *Appl. Phys. Lett.* **81** 2322 (2002)
12. Kuzyk M, in *Organic Thin Films for Waveguiding Nonlinear Optics* (Adv. in Nonlinear Optics, Vol. 3, Eds F Kajzar, J D Swalen) (Amsterdam: Gordon & Breach, 1996) p. 759
13. Boyd G T, in *Polymers for Electronic and Photonic Applications* (Ed. C P Wong) (Boston, MA: Academic Press, 1993) p. 467
14. Lee K-S, Samoc M, Prasad P N, in *Comprehensive Polymer Science* 1st Suppl. (Eds S L Aggarwal, S Russo) (Oxford: Pergamon Press, 1992) p. 407
15. Luther-Davies B, Samoc M *Curr. Opin. Solid State Mater. Sci.* **2** 213 (1997)
16. Stegeman G I, Torruellas W E *Philos. Trans. R. Soc. London A* **354** 745 (1996)
17. Zyss J (Ed.) *Molecular Nonlinear Optics*: *Materials, Physics, and Devices* (Boston: Academic Press, 1994)
18. Nalwa H S, Miyata S (Eds) *Nonlinear Optics of Organic Molecules and Polymers* (Boca Raton, FL: CRC Press, 1997)
19. Marder S R et al. *Nature* **388** 845 (1997)
20. Bertolotti M, Bowden C M, Sibilia C (Eds) *Nanoscale Linear and Nonlinear Optics*: *Intern. School on Quantum Electronics, Erice, Sicily, July 2 – 14, 2000* (AIP Conf. Proc., Vol. 560) (Melville, NY: AIP, 2001)
21. Dresselhaus M S, Dresselhaus G, Eklund P C *Science of Fullerenes and Carbon Nanotubes* (San Diego: Academic Press, 1996)
22. Endo M, Iijima S, Dresselhaus M S (Eds) *Carbon Nanotubes* (Oxford: Pergamon Press, 1996)
23. Saito R, Dresselhaus G, Dresselhaus M S *Physical Properties of Carbon Nanotubes* (London: Imperial College Press, 1998)
24. Dresselhaus M S, Dresselhaus G, Avouris P (Eds) *Carbon Nanotubes: Synthesis, Structure, Properties, and Applications* (Topics in Applied Physics, Vol. 80) (Berlin: Springer-Verlag, 2001)
25. Petričević V et al. *Appl. Phys. Lett.* **52** 1040 (1988)
26. Petričević V, Gayen S K, Alfano R R *Opt. Lett.* **14** 612 (1989)
27. Konorov S O et al. *Opt. Commun.* **224** 309 (2003)
28. Konorov S O et al. *J. Opt. A*: *Pure Appl. Opt.* (in press)
29. Akimov D A et al. *Zh. Eksp. Teor. Fiz.* **125** 247 (2004) [*JETP* **98** 220 (2004)]
30. Konorov S O et al. *J. Raman Spectrosc.* **34** 1018 (2003)
31. Konorov S O et al. *J. Raman Spectrosc.* **34** 999 (2003)
32. Konorov S O et al. *Laser Phys. Lett.* **1** 37 (2004)
33. Akimov D A et al. *J. Raman Spectrosc.* **34** 1007 (2003)
34. Konorov S O et al. *J. Opt. A*: *Pure Appl. Opt.* **5** 362 (2003)
35. Bouma B E et al. *Opt. Lett.* **21** 1839 (1996)
36. Gayen S K et al. *Appl. Opt.* **37** 5327 (1998)
37. Alfano R, Gayen S *Opt. Express* **4** 475 (1999)
38. Ivanov A A, Alfimov M V, Zheltikov A M *Laser Phys.* **10** 796 (2000)
39. Konorov S O et al., submitted
40. Akimov D A et al. *Pis'ma Zh. Eksp. Teor. Fiz.* **77** 9 (2003) [*JETP Lett.* **77** 7 (2003)]
41. Akimov D A et al. *Kvantovaya Elektron.* **33** 317 (2003) [*Quantum Electron.* **33** 317 (2003)]
42. Akimov D A et al. *Appl. Phys. B* **76** 515 (2003)
43. Konorov S O et al. *Kvantovaya Elektron.* **33** 989 (2003) [*Quantum Electron.* **33** 989 (2003)]
44. Naumov A N et al. *J. Opt. Soc. Am. B* **19** 2183 (2002)
45. Akimov D A et al. *Pis'ma Zh. Eksp. Teor. Fiz.* **74** 515 (2001) [*JETP Lett.* **74** 460 (2001)]
46. Akimov D A et al. *Appl. Phys. B* **74** 307 (2002)
47. Stanciu C et al. *Appl. Phys. Lett.* **81** 4064 (2002)
48. Akimov D A et al. *Laser Phys.* **13** 1279 (2003)
49. Golovan' L A et al. *Pis'ma Zh. Eksp. Teor. Fiz.* **78** 229 (2003) [*JETP Lett.* **78** 193 (2003)]
50. Konorov S O et al. *Appl. Phys. B* **74** (Suppl.) S145 (2002)
51. Yakovlev V V, Ivanov A, Shcheslavskiy V *Appl. Phys. B* **74** (Suppl. 1) S145 (2002)
52. Evans J M et al. *Opt. Lett.* **23** 1692 (1998)
53. Jonusauskas G, Oberle J, Rolliere C *Opt. Lett.* **23** 1918 (1998)
54. Shcheslavskiy V et al. *Appl. Opt.* **38** 3294 (1999)
55. Togashi T et al. *Appl. Phys. B* **68** 169 (1999)
56. Shen Y R *The Principles of Nonlinear Optics* (New York: J. Wiley, 1984)
57. Fejer M M et al. *IEEE J. Quantum Electron.* **28** 2631 (1992)
58. Byer R L *J. Nonlinear Opt. Phys. Mater.* **6** 549 (1997)
59. Scalora M et al. *Phys. Rev. A* **56** 3166 (1997)
60. Zheltikov A M, Tarasishin A V, Magnitskiĭ S A *Zh. Eksp. Teor. Fiz.* **118** 340 (2000) [*JETP* **91** 298 (2000)]
61. Dumeige Y et al. *Appl. Phys. Lett.* **78** 3021 (2001)
62. Knight J C et al. *Opt. Lett.* **21** 1547 (1996)
63. Knight J C et al. *Science* **282** 1476 (1998)
64. Russell P *Science* **299** 358 (2003)
65. Alfimov M V et al. *Pis'ma Zh. Eksp. Teor. Fiz.* **71** 714 (2000) [*JETP Lett.* **71** 489 (2000)]
66. Zheltikov A M *Usp. Fiz. Nauk* **170** 1203 (2000) [*Phys. Usp.* **43** 1125 (2000)]
67. Eggleton B et al. *Opt. Express* **9** 698 (2001)
68. Zheltikov A M *Usp. Fiz. Nauk* **172** 743 (2002) [*Phys. Usp.* **45** 687 (2002)]
69. Birks T A, Wadsworth W J, Russell P St J *Opt. Lett.* **25** 1415 (2000)
70. Reeves W H et al. *Opt. Express* **10** 609 (2002)
71. Broderick N G R et al. *Opt. Lett.* **24** 1395 (1999)
72. Fedotov A B et al. *Appl. Phys. B* **73** 181 (2001)
73. Fedotov A B, Yakovlev V V, Zheltikov A M *Laser Phys.* **12** 268 (2002)
74. Akimov D A et al. *Appl. Phys. B* **76** 515 (2003)
75. Naumov A N, Zheltikov A M *Opt. Express* **10** 122 (2002)
76. Fedotov A B et al. *Appl. Phys. B* **77** 313 (2003)
77. Zheltikov A M (Ed.) "Supercontinuum generation: Special issue" *Appl. Phys. B* **77** (2/3) (2003)
78. Efimov A et al. *Opt. Express* **11** 910 (2003)
79. Akimov D A et al. *Opt. Lett.* **28** 1948 (2003)
80. Zheltikov A M et al. *Zh. Eksp. Teor. Fiz.* **120** 570 (2001) [*JETP* **93** 499 (2001)]
81. Fedotov A B et al. *Kvantovaya Elektron.* **31** 387 (2001) [*Quantum Electron.* **31** 387 (2001)]
82. Zheltikov A M et al. *Kvantovaya Elektron.* **32** 542 (2002) [*Quantum Electron.* **32** 542 (2002)]
83. Fedotov A B et al. *J. Raman Spectrosc.* **33** 887 (2002)
84. Zheltikov A M *Opt. Spektrosk.* **95** 440 (2003) [*Opt. Spectrosc.* **95** 410 (2003)]
85. Zheltikov A M *Zh. Eksp. Teor. Fiz.* **124** 558 (2003) [*JETP* **97** 505 (2003)]
86. Coen S et al. *J. Opt. Soc. Am. B* **19** 753 (2002)
87. Dudley J M et al. *Opt. Express* **10** 1215 (2002)
88. Zheltikov A M, Naumov A N *Kvantovaya Elektron.* **30** 606 (2000) [*Quantum Electron.* **30** 606 (2000)]
89. Zheltikov A M, Naumov A N *Laser Phys.* **10** 887 (2000)
90. Naumov A N, Zheltikov A M *J. Raman Spectrosc.* **32** 960 (2001)
91. Naumov A N, Zheltikov A M *Appl. Phys. B* **77** 369 (2003)
92. Spano F C, Mukamel S *Phys. Rev. A* **40** 5783 (1989)
93. Knoester J *J. Chem. Phys.* **99** 8466 (1993)
94. Wang N, Chernyak V, Mukamel S *J. Chem. Phys.* **100** 2465 (1994)
95. Sheikh-Bahae M et al. *IEEE J. Quantum Electron.* **26** 760 (1990)
96. Pang Y, Samoc M, Prasad P N *J. Chem. Phys.* **94** 5282 (1991)
97. Strohkendl F P et al. *J. Opt. Soc. Am. B* **14** 92 (1997)
98. Cao X F et al. *J. Appl. Phys.* **65** 5012 (1989)
99. Minoshima K et al. *Chem. Phys. Lett.* **218** 67 (1994)
100. Johnson A E, Kumazaki S, Yoshihara K *Chem. Phys. Lett.* **211** 511 (1993)
101. Gadonas R et al. *J. Chem. Phys.* **106** 8374 (1997)
102. Gaižauskas E, Pakalnis S, Feller K-H *Chem. Phys.* **266** 69 (2001)
103. Sasaki F, Kato T, Kobayashi S *Phys. Rev. B* **63** 205411 (2001)
104. Shelkovnikov V V et al. *Khim. Vys. Energ.* **36** 295 (2002) [*High Energy Chem.* **36** 260 (2002)]
105. Scheibe G *Angew. Chem.* **49** 563 (1936)
106. Jelley E E *Nature* **138** 1009 (1936)
107. Butcher P N, Cotter D *The Elements of Nonlinear Optics* (Cambridge: Cambridge Univ. Press, 1990)
108. Reintjes J F *Nonlinear Optical Parametric Processes in Liquids and Gases* (New York: Academic Press, 1984)

109. Zheltikov A M, Koroteev N I *Usp. Fiz. Nauk* **169** 385 (1999) [*Phys. Usp.* **42** 321 (1999)]
110. Squier J et al. *Opt. Express* **3** 315 (1998)
111. Yelin D, Silberberg Y *Opt. Express* **5** 169 (1999)
112. Sidorov-Biryukov D A et al. *Kvantovaya Elektron.* **30** 1080 (2000) [*Quantum Electron.* **30** 1080 (2000)]
113. Xie R-H, Jiang J *Appl. Phys. Lett.* **71** 1029 (1997)
114. Wan X, Dong J, Xing D Y *Phys. Rev. B* **58** 6756 (1998)
115. Jiang J, Dong J M, Xing D Y *Phys. Rev. B* **59** 9838 (1999)
116. Margulis Vl A, Gaiduk E A, Zhidkin E N *Diamond Relat. Mater.* **8** 1240 (1999)
117. Slepyan G Ya et al. *Phys. Rev. A* **60** R777 (1999)
118. Slepyan G Ya et al. *Phys. Rev. A* **63** 053808 (2001)
119. Vivien L et al. *Chem. Phys. Lett.* **307** 317 (1999)
120. Jin Z et al. *Chem. Phys. Lett.* **318** 505 (2000)
121. Riggs J E et al. *J. Phys. Chem. B* **104** 7071 (2000)
122. Vivien L et al. *IEEE J. Quantum Electron.* **36** 680 (2000)
123. Vivien L et al. *J. Nonlinear Opt. Phys. Mater.* **9** 297 (2000)
124. Sun X et al. *Appl. Opt.* **39** 1998 (2000)
125. Liu X et al. *Appl. Phys. Lett.* **74** 164 (1999)
126. De Dominicis L et al., in *Abstracts of European Conf. on Nonlinear Optical Spectroscopy, March 30 – April 1, 2003, Besançon, France*, p. 15
127. Wang S et al. *Chem. Phys. Lett.* **320** 411 (2000)
128. Chen Y-C et al. *Appl. Phys. Lett.* **81** 975 (2002)
129. Botti S et al. *Appl. Phys. Lett.* **80** 1441 (2002)
130. Botti S et al. *Chem. Phys. Lett.* **355** 395 (2002)
131. Hafner J H et al. *Chem. Phys. Lett.* **296** 195 (1998)
132. Cheng H M et al. *Chem. Phys. Lett.* **289** 602 (1998)
133. Bachilo S M et al. *Science* **298** 2361 (2002)
134. Rao A M et al. *Science* **275** 187 (1997)
135. Du D, Liu X, Mourou G *Appl. Phys. B* **63** 617 (1996)
136. Tien A-C et al. *Phys. Rev. Lett.* **82** 3883 (1999)
137. Lenzner M et al. *Phys. Rev. Lett.* **80** 4076 (1998)
138. Damnjanovic M et al. *Phys. Rev. B* **60** 2728 (1999)
139. Shkurinov A P, Dubrovskii A V, Koroteev N I *Phys. Rev. Lett.* **70** 1085 (1993)
140. Fischer P et al. *Phys. Rev. Lett.* **85** 4253 (2000)
141. Belkin M A et al. *Phys. Rev. Lett.* **85** 4474 (2000)
142. Belkin M A et al. *Phys. Rev. Lett.* **87** 113001 (2001)
143. Akhmanov S A, Koroteev N I *Metody Nelineĭnoĭ Optiki v Spektroskopii Rasseyaniya Sveta*: *Aktivnaya Spektroskopiya Rasseyaniya Sveta* (Methods of Nonlinear Optics in Light Scattering Spectroscopy: Active Spectroscopy of Light Scattering) (Moscow: Nauka, 1981)
144. Eesley G L *Coherent Raman Spectroscopy* (Oxford: Pergamon Press, 1981)
145. Govorkov S V et al. *Opt. Lett.* **16** 1013 (1991)
146. Govorkov S V et al. *J. Lumin.* **53** 153 (1992)
147. Voisin C et al. *J. Phys. Chem. B* **105** 2264 (2001)
148. Yang N, Angerer W E, Yodh A G *Phys. Rev. A* **64** 045801 (2001)
149. Srivastava A, Eisenthal K B *Chem. Phys. Lett.* **292** 345 (1998)
150. Hartings J M et al. *Chem. Phys. Lett.* **281** 389 (1997)
151. Duncan M D, Reintjes J, Manuccia T J *Opt. Lett.* **7** 350 (1982)
152. Zumbusch A, Holton G R, Sunney Xie X *Phys. Rev. Lett.* **82** 4142 (1999)
153. Akimov D A et al. *Proc. SPIE* **4749** 101 (2002)
154. Puppels G J, Grond M, Greve J *Appl. Spectrosc.* **47** 1256 (1993)
155. Rosasco G J, Etz E S, Cassat W A *Appl. Spectrosc.* **29** 396 (1975)
156. Konorov S O et al. *Appl. Phys. B* **78** 73 (2004)
157. Lambrecht W R L et al. *Phys. Status Solidi B* **202** 5 (1997)
158. Harris G L (Ed.) *Properties of Silicon Carbide* (EMIS Datareviews Series, No. 13) (London: INSPEC, Institution of Electrical Engineers, 1995)
159. Choyke W J, Hamilton D R, Patrick L *Phys. Rev.* **133** A1163 (1964)
160. Logothetidis S, Petalas J *J. Appl. Phys.* **80** 1768 (1996)
161. Lambrecht W R L et al. *Phys. Rev. B* **50** 10722 (1994)
162. Powell J A *J. Opt. Soc. Am.* **62** 341 (1972)
163. Adolph B et al. *Phys. Rev. B* **55** 1422 (1997)
164. Käckell P, Wenzien B, Bechstedt F *Phys. Rev. B* **50** 10761 (1994)
165. Backes W H, Bobbert P A, van Haeringen W *Phys. Rev. B* **51** 4950 (1995)
166. Adolph B et al. *Phys. Rev. B* **53** 9797 (1996)
167. Chen J, Levine Z H, Wilkins J W *Phys. Rev. B* **50** 11514 (1994)
168. Feurer T, Glass A, Sauerbrey R *Appl. Phys. B* **65** 295 (1997)
169. Rashkeev S N, Lambrecht W R L, Segall B *Phys. Rev. B* **57** 9705 (1998)
170. Adolph B, Bechstedt F *Phys. Rev. B* **62** 1706 (2000)
171. Niedermeier S et al. *Appl. Phys. Lett.* **75** 618 (1999)
172. Lawand N M et al. *Nature* **368** 436 (1994)
173. Sha W L, Liu C-H, Alfano R R *Opt. Lett.* **19** 1922 (1994)
174. Cao H et al. *Phys. Rev. Lett.* **82** 2278 (1999)
175. Golovan L A et al. *Appl. Phys. B* **73** 31 (2001)
176. Kashkarov P K et al. *J. Opt. Soc. Am. B* **19** 2273 (2002)
177. Golovan L A et al. *Appl. Phys. B* **76** 429 (2003)
178. Jones D J et al. *Science* **288** 635 (2000)
179. Holzwarth R et al. *Phys. Rev. Lett.* **85** 2264 (2000)
180. Baltuska A, Fuji T, Kobayashi T *Opt. Lett.* **27** 1241 (2002)
181. Hartl I et al. *Opt. Lett.* **26** 608 (2001)
182. Konorov S O, Zheltikov A M *Opt. Express* **11** 2440 (2003)
183. Fedotov A B et al. *J. Raman Spectrosc.* **33** 888 (2002)
184. Kravtsov V E, Agranovich V M, Grigorishin K I *Phys. Rev. B* **44** 4931 (1991)
185. Kurtz S K, Perry T T *J. Appl. Phys.* **39** 3798 (1968)
186. Ishimaru A *Wave Propagation and Scattering in Random Media* (New York: Academic Press, 1995)
187. Anderson R R, Parrish J A *J. Invest. Dermatol.* **77** 13 (1981)
188. Schmitt J M, Yadlowsky M J, Bonner R F *Dermatology* **191** 93 (1995)
189. Fujimoto J G et al. *Nature Med.* **1** 972 (1995)
190. Feldchtein F I et al. *Opt. Express* **1** 432 (1997)
191. Feldchtein F I et al. *Opt. Express* **3** 257 (1998)
192. Feldchtein F I et al. *Opt. Express* **3** 239 (1998)
193. Huang D et al. *Science* **254** 1178 (1991)
194. Schmitt J M et al. *Phys. Med. Biol.* **39** 1705 (1994)
195. Tearney G J et al. *Opt. Lett.* **21** 1408 (1996)
196. Gayen S K et al. *Lasers Life Sci.* **8** 187 (1999)
197. Peleg G et al. *Bioimaging* **4** 215 (1996)
198. Barad Y et al. *Appl. Phys. Lett.* **70** 922 (1997)
199. Müller M et al. *J. Microsc.* **191** 266 (1998)
200. Squier J A et al., in *XIth Intern. Conf. on Ultrafast Phenomena, Garmish, Germany, 11 – 17 July 1998*, Technical Digest (München: Inst. Medizinische Optik, 1998) p. 156
201. Kuditcher A et al., in *CLEO'98 — Conf. on Lasers and Electro-Optics, San Francisco, CA, USA, May 3 – 8, 1998* (Technical Digest Series, Vol. 6) (Washington, DC: Optical Society of America, 1998) p. 233
202. Ivanov A A et al. *Laser Phys.* **11** 158 (2001)
203. Dürr H, Bouas-Laurent H (Eds) *Photochromism*: *Molecules and Systems* (Studies in Organic Chemistry, Vol. 40) (Amsterdam: Elsevier, 1990)
204. Brown G H (Ed.) *Photochromism* (Techniques of Chemistry, Vol. 3) (New York: Wiley-Interscience, 1971)
205. Barachevskiĭ V A, Lashkov G I, Tsekhomskiĭ V A *Fotokhromizm i Ego Primeneniya* (Photochromism and Its Applications) (Moscow: Khimiya, 1977)
206. Berkovic G, Krongauz V, Weiss V *Chem. Rev.* **100** 1741 (2000)
207. Asanuma H et al. *Chem. Lett.* (2) 108 (2001)
208. Ernsting N P, Arthen-Engeland Th *J. Phys. Chem.* **95** 5502 (1991)
209. Zhang J Z et al. *J. Am. Chem. Soc.* **114** 10921 (1992)
210. Antipin S A et al. *Chem. Phys. Lett.* **331** 378 (2000)
211. Konorov S O et al. *Pis'ma Zh. Eksp. Teor. Fiz.* **78** 281 (2003) [*JETP Lett.* **78** 246 (2003)]
212. Konorov S O et al. *Chem. Phys. Lett.* **381** 572 (2003)
213. Kohler B et al. *Phys. Rev. Lett.* **74** 3360 (1995)
214. Bardeen C J, Wang Q, Shank C V *Phys. Rev. Lett.* **75** 3410 (1995)